FEDERAL UNIVERSITY OF JUIZ DE FORA
FACULTY OF ENGINEERING
GRADUATE PROGRAM IN BUILT ENVIRONMENT

Júlia Martins Carrara

Performance analysis of modular units used in non-load-bearing masonry: a comparative study between the cities of Juiz de Fora (Brazil) and Santa Fe (Argentina)

Juiz de Fora
2026

Júlia Martins Carrara

Performance analysis of modular units used in non-load-bearing masonry: a comparative study between the cities of Juiz de Fora (Brazil) and Santa Fe (Argentina)

Dissertation submitted to the Graduate Program in Built Environment of the Federal University of Juiz de Fora in partial fulfillment of the requirements for the degree of Master in Built Environment. Area of concentration: Built Environment.

Advisor: Prof. Dr. Maria Teresa Gomes Barbosa

Co-advisor: Prof. Dr. Anabela Guadalupe Guilarducci

Juiz de Fora

2026

Júlia Martins Carrara

Performance analysis of the modular components used in the construction of infill masonry: a comparative study between the cities of Juiz de Fora (Brazil) and Santa Fe (Argentina)

Dissertação apresentada ao Programa de Pós-graduação em Ambiente Construído da Universidade Federal de Juiz de Fora como requisito parcial à obtenção do título de Mestre em Ambiente Construído. Área de concentração: Ambiente Construído

Aprovada em 09 de novembro de 2026.

BANCA EXAMINADORA

Profa. Dra. Maria Teresa Gomes Barbosa - Orientadora
Universidade Federal de Juiz de Fora

Profa. Dra. Anabela Guadalupe Guilharducci
Universidad Tecnológica Nacional - UTN Santa Fé

Profa. Dra. Maria Ávila Branquinho
Universidade Federal de Juiz de Fora

Profa. Ma. Dianela González
Universidad Tecnológica Nacional - UTN Santa Fé

Juiz de Fora, 16/11/2026.

Documento assinado eletronicamente por **Maria Teresa Gomes Barbosa**, **Professor(a)**, em 16/11/2026, às 16:55, conforme horário oficial de Brasília, com fundamento no § 3º do art. 4º do Decreto nº 10.543, de 13 de novembro de 2020.

Documento assinado eletronicamente por **Dianela Guadalupe Gonzalez**, **Usuário Externo**, em 16/11/2026, às 18:43, conforme horário oficial de Brasília, com fundamento no § 3º do art. 4º do Decreto nº 10.543, de 13 de novembro de 2020.

Documento assinado eletronicamente por **Anabela Guilarducci**, **Usuário Externo**, em 18/11/2026, às 10:02, conforme horário oficial de Brasília, com fundamento no § 3º do art. 4º do Decreto nº 10.543, de 13 de novembro de 2020.

Documento assinado eletronicamente por **Maria Avila Branquinho**, **Professor(a)**, em 18/11/2026, às 10:38, conforme horário oficial de Brasília, com fundamento no § 3º do art. 4º do Decreto nº 10.543, de 13 de novembro de 2020.

A autenticidade deste documento pode ser conferida no Portal do SEI-Ufjf (www2.ufjf.br/SEI) através do ícone Conferência de Documentos, informando o código verificador **3353143** e o código CRC **381EB982**.

ACKNOWLEDGMENTS

No work can be accomplished without the support of people and institutions that, each in their own way, contribute to such remarkable moments. I am grateful:

To God, for being a source of faith and protection throughout my academic journey.

To my parents, Marcilia and Jovani, for all their love, support and encouragement, for dreaming alongside me and always trusting in my potential.

To my twin sister, Marcela, for her daily companionship, her encouragement and for sharing every step of this journey with me.

To my advisor, Maria Teresa, for the trust placed in me, for her warmth, kindness and the opportunity to work together. My eternal gratitude.

To my co-advisor, Anabela, for her support and for all the cooperation in the development of this research.

To the Federal University of Juiz de Fora (UFJF), especially the Graduate Program in Built Environment (PROAC), for the technical support essential to this research.

To the Universidad Tecnológica Nacional - UTN Santa Fe, for the exchange of ideas, the collaboration and the partnership.

To the Coordination for the Improvement of Higher Education Personnel – Brazil (CAPES), for the financial support that made this research possible.

To the Civil Construction Materials Laboratory, for the technical support essential to the development of this research, with special thanks to the technician Romilda Prata for her collaboration and availability.

To the Strength of Materials Laboratory, represented by Prof. Dr. Gustavo Henrique Nalon, for his valuable contributions, technical support and constant availability.

To the Chemistry Laboratory and to NEEM – Center for Spectroscopy and Molecular Structure, represented by Prof. Dr. Luiz Fernando Cappa de Oliveira and M.Sc. Patrick de Souza de Carvalho, for the support, collaboration and cooperation provided throughout the development of this dissertation.

To my friends from Liga UFJFck, for welcoming the team's only architect.

To the friends I have made at every stage of my life and to the family members who cheer for and celebrate my achievements.

RESUMO

A seleção de componentes modulares empregados na confecção de alvenarias de vedação exerce influência direta no desempenho térmico das edificações e, consequentemente, no conforto dos usuários e na eficiência energética. Nesse contexto, este estudo tem como objetivo investigar as propriedades dos materiais de construção utilizados em sistemas de vedação, com ênfase na alvenaria, mais especificamente nos sistemas modulares (bloco cerâmico e bloco de concreto). O procedimento experimental consistiu em ensaios laboratoriais, conforme a normalização brasileira e argentina, nos quais foram avaliadas as propriedades macroscópicas dos elementos monolíticos comumente empregados nas cidades de Juiz de Fora (MG, Brasil) e Santa Fé (Santa Fé, Argentina), bem como a caracterização microestrutural e mineralógica desses materiais por meio de microscopia eletrônica de varredura (MEV) e espectroscopia Raman, e a caracterização térmica por análises termogravimétrica e térmica diferencial (TGA/DTA), sendo também determinadas a condutividade e a resistência térmica pelo método do medidor de fluxo de calor. Os resultados evidenciaram diferenças relevantes entre os materiais e contextos regionais analisados, a saber, os blocos cerâmicos argentinos apresentaram menor massa específica aparente e menor absorção de água que os brasileiros, características favoráveis ao desempenho térmico, porém resistência à compressão inferior enquanto que os blocos de concreto argentinos se destacaram pelas propriedades mecânicas superior à observada no Brasil, apesar de apresentarem menor massa específica aparente e maior absorção de água. As análises microscópicas e de condutividade térmica corroboram com os resultados, evidenciando que os cerâmicos possuem características favoráveis ao desempenho térmico e com boa concordância com as prescrições normativas. Finalmente, conclui-se que o desempenho dos blocos de vedação depende não apenas do tipo de material, mas, também, da matéria-prima e do processo produtivo de cada região, o que reforça a importância da caracterização experimental local na especificação de materiais, bem como é apresentado subsídios para a harmonização entre as normas técnicas no âmbito do Mercosul.

Palavras-chave: materiais de construção; desempenho; habitabilidade; eficiência energética; sustentabilidade.

ABSTRACT

The selection of modular units used in non-load-bearing masonry directly influences the thermal performance of buildings and, consequently, user comfort and energy efficiency. In this context, this study aimed to investigate the properties of construction materials used in wall systems, with emphasis on masonry, and more specifically on modular systems (ceramic blocks and concrete blocks). The experimental procedure consisted of laboratory tests carried out in accordance with Brazilian and Argentine standards, in which the macroscopic properties of the monolithic units commonly used in the cities of Juiz de Fora (MG, Brazil) and Santa Fe (Santa Fe, Argentina) were evaluated, together with the microstructural and mineralogical characterization of these materials by scanning electron microscopy (SEM) and Raman spectroscopy, and their thermal characterization by thermogravimetric and differential thermal analysis (TGA/DTA); thermal conductivity and thermal resistance were also determined by the heat flow meter method. The results revealed relevant differences between the materials and regional contexts analyzed: the Argentine ceramic blocks showed lower apparent density and lower water absorption than the Brazilian ones, characteristics favorable to thermal performance, but lower compressive strength, whereas the Argentine concrete blocks stood out for mechanical properties superior to those observed in Brazil, despite their lower apparent density and higher water absorption. The microscopic and thermal conductivity analyses corroborate these results, showing that the ceramic blocks have characteristics favorable to thermal performance and good agreement with the standard prescriptions. Finally, it is concluded that the performance of non-load-bearing blocks depends not only on the type of material but also on the raw materials and production process of each region, which reinforces the importance of local experimental characterization in the specification of materials; inputs for the harmonization of technical standards within Mercosur are also presented.

Keywords: construction materials; performance; habitability; energy efficiency; sustainability.

LIST OF FIGURES

Figure 1 – Energy consumption 12
Figure 2 – Classification of building insulation materials 13
Figure 3 – Annual variation of minimum and maximum temperatures in the cities of Santa Fe and Juiz de Fora 16
Figure 4 – Thermal performance assessment methods 26
Figure 5 – Map of Brazil with the 8 bioclimatic zones 28
Figure 6 – Location of the cities of Juiz de Fora and Santa Fe 35
Figure 7 – Methodological flowchart 44
Figure 8 – Magnifications of 50x, 250x, 500x, 1,000x and 2,000x of BC BR 46
Figure 9 – Magnifications of 50x, 250x, 500x, 1,000x and 2,000x of BC AR 48
Figure 10 – Raman spectra of BC BR normalized to the 148 cm^{-1} band 51
Figure 11 – Raman spectrum of BC AR normalized to the 145 cm^{-1} band 53
Figure 12 – TGA and DTA curves of BC BR 57
Figure 13 – TGA and DTA curves of BC AR 58
Figure 14 – Magnifications of 50x, 250x, 500x, 1,000x and 2,000x of BCC BR 67
Figure 15 – Magnifications of 50x, 250x, 500x, 1,000x and 2,000x of BCC AR 68
Figure 16 – Raman spectra of the BCC BR samples normalized to the 1086 cm^{-1} band 72
Figure 17 – Raman spectra of BCC AR normalized to the 1086 cm^{-1} band 74
Figure 18 – TGA and DTA curves of BCC BR 78
Figure 19 – TGA and DTA curves of BCC AR 80

LIST OF TABLES

Table 1 – Admissible thermal transmittance, thermal lag and solar heat gain factor for each type of external wall 29
Table 2 – Thermal properties of materials 29
Table 3 – Properties of materials according to IRAM 11601 30
Table 4 – Kmaxadm values for winter conditions in W/m²·K 31
Table 5 – Maximum thermal transmittance values for walls under summer conditions in W/m²·K 32
Table 6 – Comparative summary of Brazilian and Argentine standards 33
Table 7 – Tests for the evaluation of the properties of each block and their respective standards 40
Table 8 – Mean results of the tests performed on the BC 44
Table 9 – Summary of the analysis of macroscopic vs. SEM results for BC BR vs. BC AR 49
Table 10 – Assignment of the Raman bands observed in the spectra of the BC BR samples investigated 51
Table 11 – Interpretation of the BC BR band assignments 52
Table 12 – Assignment of the Raman bands observed in the spectra of the BC AR sample investigated 54
Table 13 – Interpretation of the BC AR band assignments 54
Table 14 – Summary of the analysis of macroscopic vs. Raman results for BC BR vs. BC AR 55
Table 15 – Summary of the analysis of macroscopic vs. thermogravimetric results for BC BR vs. BC AR 60
Table 16 – Mean thermal resistance result of BC AR (heat flow meter method) 62
Table 17 – Summary of the analysis of macroscopic vs. thermal conductivity results for BC BR vs. BC AR 63
Table 18 – Data from the tests performed on BCC BR vs. BCC AR 66
Table 19 – Summary of the analysis of macroscopic vs. SEM results for BCC BR vs. BCC AR 70
Table 20 – Assignment of the Raman bands observed in the spectra of the BCC BR samples investigated 72
Table 21 – Interpretation of the BCC BR band assignments 73

Table 22 – Assignment of the Raman bands observed in the spectra of BCC AR 75
Table 23 – Interpretation of the BCC AR band assignments 75
Table 24 – Summary of the analysis of macroscopic vs. Raman results for BCC BR vs. BCC AR.....77
Table 25 – Summary of the analysis of macroscopic vs. thermogravimetric results for BCC BR vs. BCC AR.....81
Table 26 – Mean thermal conductivity and thermal resistance results of the concrete blocks (heat flow meter method) 84
Table 27 – Summary of the analysis of macroscopic vs. thermal conductivity results for BCC BR vs. BCC AR.....86
Table 28 – Comparative synthesis of the four materials studied: macroscopic, microscopic and thermal tests 88

LIST OF ABBREVIATIONS AND ACRONYMS

ABNT	Brazilian Association of Technical Standards
AR	Argentina
ASTM	American Society for Testing and Materials
BC	Ceramic Block
BCC	Concrete Block
BR	Brazil
CBCS	Brazilian Council for Sustainable Construction
CECOVI	Centro de Investigación y Desarrollo para la Construcción y la Vivienda
CIRSOC	Centro de Investigación de los Reglamentos Nacionales de Seguridad para las Obras Civiles
CV	Coefficient of Variation
DTA	Differential Thermal Analysis
HFM	Heat Flow Meter
IBGE	Brazilian Institute of Geography and Statistics
INDEC	National Institute of Statistics and Censuses (Argentina)
IRAM	Argentine Institute for Standardization and Certification
ISO	International Organization for Standardization
SEM	Scanning Electron Microscopy
NBR	Brazilian Standard
NEEM	Center for Spectroscopy and Molecular Structure
NIST	National Institute of Standards and Technology
SDG	Sustainable Development Goal
UN	United Nations
PMJF	Juiz de Fora City Hall
TGA	Thermogravimetric Analysis
UFJF	Federal University of Juiz de Fora
UTN	Universidad Tecnológica Nacional - Santa Fe

LIST OF SYMBOLS

AA	Water absorption
c	Specific heat
$Ca(OH)_2$	Calcium hydroxide (portlandite)
°C	Degree Celsius
cm	Centimeter
cm^{-1}	Reciprocal centimeter (wavenumber unit)
CO_2	Carbon dioxide
CO_3^{2-}	Carbonate ion
C-S-H	Calcium silicate hydrate
f_{bk}	Compressive strength
F_{So}	Solar factor
g	Gram
h	Hour
K	Kelvin
kg	Kilogram
kJ	Kilojoule
km	Kilometer
km/h	Kilometer per hour
K_{maxadm}	Maximum admissible thermal transmittance
kN	Kilonewton
kPa	Kilopascal
L	Specimen thickness
m	Meter
m^2	Square meter
m^3	Cubic meter
mg	Milligram
min	Minute
mm	Millimeter
MPa	Megapascal
N_2	Nitrogen

nm	Nanometer
Q/A	Heat flux per unit area
R	Thermal resistance
SO_4^{2-}	Sulfate ion
TiO_2	Titanium dioxide (anatase)
T_m	Mean test temperature
U	Thermal transmittance
W	Watt
δ	Bending (vibrational mode)
ΔT	Temperature difference
λ	Thermal conductivity
v	Wavenumber
v_{as}	Antisymmetric stretching
v_s	Symmetric stretching
ρ	Apparent density (standard values)
$ρ_{ap}$	Apparent density
φ	Thermal lag
%	Percentage

CONTENTS

1 INTRODUCTION 15
1.1 OBJECTIVES 20
1.2 RELEVANCE AND IMPACTS 20
1.3 STATEMENT ON THE USE OF ARTIFICIAL INTELLIGENCE 21
1.4 STRUCTURE OF THE DISSERTATION 21
2 THERMAL PERFORMANCE OF WALL SYSTEMS AND ENERGY EFFICIENCY OF BUILDINGS 22
2.1 INITIAL CONSIDERATIONS 22
2.2 THERMAL CHARACTERISTICS OF CONSTRUCTION MATERIALS 23
3 STANDARD PRESCRIPTIONS ON THERMAL COMFORT 26
3.1 BRAZILIAN STANDARDS 26
3.2 ARGENTINE STANDARDS 29
3.3 COMPARATIVE ANALYSIS OF THE STANDARDS 32
4 MATERIALS AND METHODS 34
4.1 INITIAL CONSIDERATIONS 34
4.1.1 **The city of Juiz de Fora** 35
4.1.2 **The city of Santa Fe** 35
4.2 MATERIALS 36
4.2.1 **Ceramic block** 37
4.2.2 **Concrete block** 37
4.3 METHODS 38
4.3.1 **Stage 1 - Evaluation of macroscopic properties** 38
4.3.2 **Stage 2 - Evaluation of microscopic and thermal properties** 39
5 RESULTS AND ANALYSES 43
5.1 CERAMIC BLOCKS 43
5.1.1 **Macroscopic tests** 43
i) BC BR 43
ii) BC AR 43
iii) BC BR vs. BC AR 44
5.1.2 **Scanning Electron Microscopy (SEM)** 44
i) BC BR 44
ii) BC AR 46
iii) BC BR vs. BC AR 47
5.1.3 **Raman Spectroscopy** 49
i) BC BR 49
ii) BC AR 51

iii) BC BR vs. BC AR 52
5.1.4 **Thermogravimetry** 54
i) BC BR 54
ii) BC AR 55
iii) BC BR vs. BC AR 56
5.1.5 **Thermal conductivity** 58
i) BC BR 58
ii) BC AR 58
iii) BC BR vs. BC AR 59
5.1.6 **Summary of Results** 60
5.2 CONCRETE BLOCKS (BCC) 61
5.2.1 **Macroscopic tests** 61
i) BCC BR 61
ii) BCC AR 62
iii) BCC BR vs. BCC AR 62
5.2.2 **Scanning Electron Microscopy (SEM)** 63
i) BCC BR 63
ii) BCC AR 64
iii) BCC BR vs. BCC AR 65
5.2.3 **Raman Spectroscopy** 67
i) BCC BR 67
ii) BCC AR 70
iii) BCC BR vs. BCC AR 72
5.2.4 **Thermogravimetry** 74
i) BCC BR 74
ii) BCC AR 75
iii) BCC BR vs. BCC AR 76
5.2.5 **Thermal conductivity** 78
i) BCC BR 78
ii) BCC AR 79
iii) BCC BR vs. BCC AR 79
5.2.6 **Summary of results** 81
5.3 ANALYSES 82
6 CONCLUSIONS 86
7 REFERENCES 92

1 INTRODUCTION

Thermal comfort in the built environment plays a very important role in users' lives, as it contributes to the full performance of their daily tasks and to their well-being (Klamt *et al.*, 2024). Moreover, understanding the conditions and parameters associated with the habitability requirements of buildings, and more specifically the selection of wall materials and components, becomes essential to respond satisfactorily to different climatic conditions and to the needs of users in different locations (Oliveira, Rupp and Ghisi, 2020).

According to the Global Status Report for Buildings and Construction (UNEP, 2024), published by the United Nations Environment Programme, the building and construction sector accounted for approximately 30% of final energy demand, mainly due to operational needs such as heating, cooling and lighting. When the energy consumption associated with the production of construction materials is also considered, this share rises to 34% of global demand (Figure 1).

Figure 1 – Energy consumption.

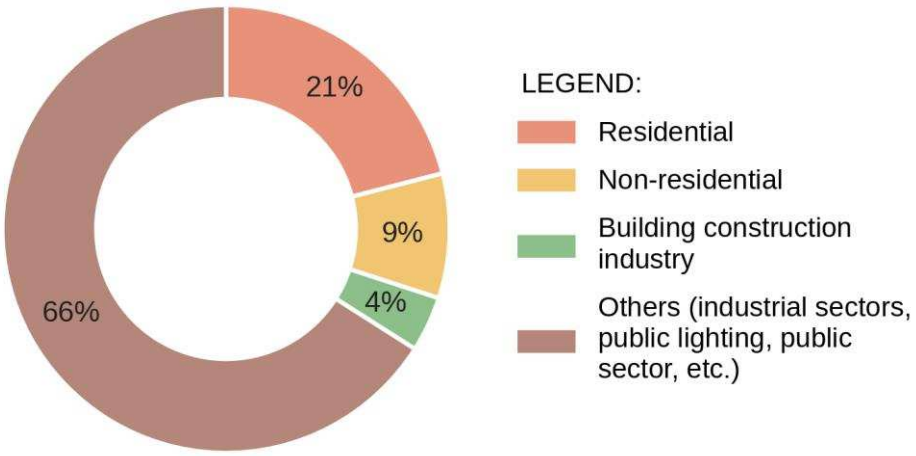

Source: Adapted (2026) from UNEP (2024).

Given the significant impact of buildings (residential or not) on global CO_2 emissions, energy efficiency is of utmost importance for sustainability and for saving the planet's resources. In this context, choosing construction materials and components according to their thermal properties and applications emerges as a strategy capable of improving thermal comfort, promoting energy efficiency and

reducing the need for artificial air-conditioning systems (Kohl, Silva and Ribeiro, 2023), in addition to significantly improving users' quality of life (Cruz, 2020).

According to Durakovic, Yildiz and Yahia (2020), the range of materials that improve thermal comfort in buildings is broad and constantly evolving, as shown in Figure 2, and building insulation materials are divided into two groups: inorganic and organic materials.

Figure 2 – Classification of building insulation materials.

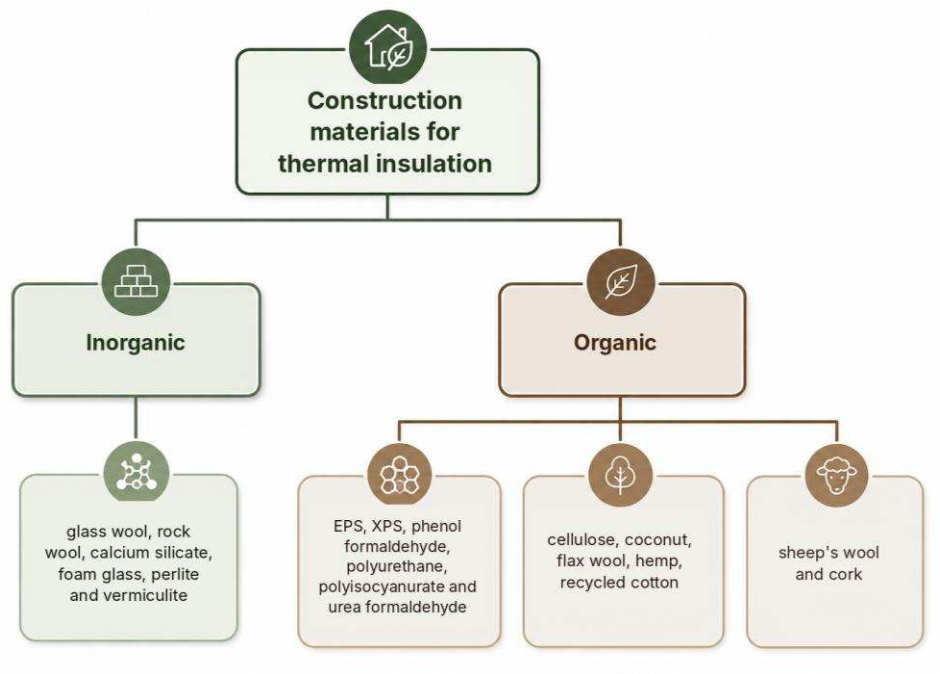

Source: Adapted (2026) from Durakovic, Yildiz and Yahia (2020) and generated with ChatGPT-5.6 Luna (2026).

It should be noted that the thermal performance of the building envelope should not be understood only through steady-state analyses, but also from a dynamic perspective that considers the response of materials to thermal variations throughout the day and the seasons (El-Bichri *et al.*, 2022). Parameters such as thermal inertia, thermal lag and damping of temperature oscillations are particularly relevant in buildings exposed to climates with a high daily temperature range, and they are directly influenced by the physical and structural properties of the wall materials (Ortlepp and Satanova, 2025).

Based on this understanding, the international literature indicates that the microstructure of wall materials plays a decisive role in the thermal performance of external walls (Ortlepp and Satanova, 2025). In porous materials such as ceramic and

concrete blocks, the distribution, size and connectivity of pores directly influence the effective thermal conductivity (Schiller *et al*., 2019). This influence explains the variability observed in the thermal properties of materials and highlights the need for detailed experimental analyses (El-Bichri *et al*., 2022).

Some materials used in construction, such as ceramic blocks and concrete blocks, have different thermal characteristics and properties, which directly affects the thermal comfort of buildings.

Regarding building components, Alhaddad and Jun (2013) evaluated systems made of mud bricks, fired bricks, stone and concrete bricks in Sana'a (capital of Yemen), and found that mud bricks performed best thermally under local climatic conditions. Elias-Ozkan *et al*. (2005) carried out a comparative analysis of different building systems, including traditional mud-brick masonry, straw-bale construction, prefabricated buildings made of thin concrete sandwich panels, and aerated concrete and reinforced concrete structures in Central Anatolia (Turkey). The authors concluded that the systems based on straw bales and mud bricks performed better in terms of thermal comfort and energy efficiency, standing out as alternatives better suited to local climatic conditions.

Passive cooling provided by construction materials is a strategy aimed at improving the thermal performance of buildings while meeting sustainability criteria, since it is economical, ecological and adaptable to local climatic conditions (Suryo, 2019). Therefore, it is of utmost importance to evaluate the properties of each material, since the choice does not depend solely on thermal performance.

The microstructure of wall materials is directly associated with the production processes adopted in their manufacture (El-Bichri *et al*., 2022). Differences in raw material composition, particle size distribution and forming methods result in significant changes in the apparent density and porosity of the blocks (Suryo, 2019). These changes affect the thermal performance of external walls, reinforcing the importance of considering the production context of materials when evaluating the building envelope (Mansouri and Leila, 2023).

Considering that production processes and raw materials vary regionally, international studies highlight the relevance of analyzing locally produced construction materials (Mansouri and Leila, 2023). The use of regional materials can contribute to improving the thermal performance of buildings and to reducing the environmental impacts associated with transportation and industrialization (Fati et al., 2020). In this

sense, the thermal characterization of the materials actually used in each region becomes essential for the development of building solutions adapted to local climatic conditions (Balaji, Mani and Reddy, 2014).

The thermal performance of the envelope is directly reflected in the thermal comfort conditions inside buildings, influencing the stability of indoor temperatures throughout the day. Wall materials with suitable thermal properties are able to damp external temperature variations, reducing thermal discomfort and dependence on active air-conditioning systems (Balaji, Mani and Reddy, 2014). Thus, the careful choice of envelope materials contributes both to energy efficiency and to users' well-being (Fati et al., 2020).

Despite advances in the international literature on the thermal performance of wall materials, investigations that systematically integrate material properties, production processes and different climatic contexts are still limited (El-Bichri *et al*., 2022). This limitation is particularly evident in comparative studies involving materials widely used in South America, such as ceramic and concrete blocks (Suryo, 2019). Therefore, investigations that simultaneously consider climate and regional production become essential for advancing technical knowledge in the region (Mansouri and Leila, 2023).

Brazil is a country with a large territory and great climatic diversity due to differences in relief, altitude, air mass dynamics and ocean currents (Barbosa, Aguilar and Sales, 2021). NBR 15220-3 (ABNT, 2024) is the thermal performance standard that defines requirements based on local climatic conditions and minimum thermal performance for comfortable occupancy, and it presents eight categories of bioclimatic zones for the climates of 330 cities in the country, with their respective guidelines (Barbosa, Aguilar and Sales, 2021). The city of Juiz de Fora is in bioclimatic zone 3, for which the recommended external wall type is a light reflective wall with a light insulated roof (ABNT, 2024).

Argentina, in turn, is influenced by factors such as latitude, altitude, proximity to the Atlantic and Pacific Oceans and the presence of the Andes mountain range (World Bank Group, 2021). Santa Fe, capital of the province of Santa Fe, is located on a low-lying plain bordered by the Paraná and El Salado-Juramento rivers and has a humid climate (Venturini, 2022). Several standards of the Instituto Argentino de Normalización y Certificación (IRAM) address the thermal conditioning of buildings: IRAM 11601 (IRAM, 2004), which defines the thermal properties of the most commonly

used construction materials; IRAM 11605 (IRAM, 2002), which defines maximum admissible thermal transmittance values for different building components, such as walls, roofs and floors; and IRAM 11900 (IRAM, 2019), which establishes a methodology for evaluating and rating the energy efficiency of buildings.

However, building typologies that disregard regional climatic issues still predominate in construction, with aesthetic aspects prioritized over the technical issues of each location, as exemplified by the glass curtain walls of commercial buildings (Barbosa, Aguilar and Sales, 2021).

In view of the above, this research aims to investigate the thermal properties of materials such as ceramic blocks and concrete blocks manufactured in the city of Juiz de Fora (Minas Gerais – Brazil) and in the city of Santa Fe (Argentina), in order to enable a comparative analysis and to strengthen knowledge about construction materials, their properties and their behavior in different climatic regions and regional contexts, whose annual temperatures are presented in Figure 3.

Figure 3 – Annual variation of minimum and maximum temperatures in the cities of Santa Fe and Juiz de Fora.

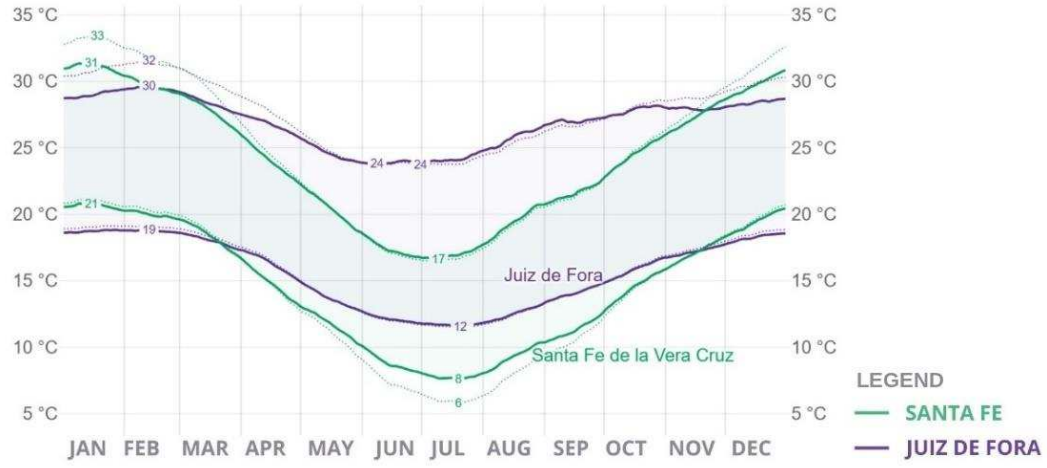

Source: Adapted (2026) from Weather Spark (2018).

Despite the widespread use of ceramic blocks and concrete blocks in wall systems in South America, comparative studies correlating experimental thermal properties, microstructure and standard compliance in different regional climatic contexts are still scarce.

1.1 OBJECTIVES

The main objective of this work is to investigate the thermal properties of the construction materials used in building walls, more specifically in the masonry of buildings located in the cities of Juiz de Fora (MG – Brazil) and Santa Fe (Santa Fe – Argentina).

The specific objectives of this work are:

i) To evaluate the thermal properties of the materials from Brazil and Argentina, namely ceramic blocks and concrete blocks, by determining thermal conductivity and thermal resistance with the heat flow meter method.

ii) To evaluate the macroscopic properties of the materials studied through apparent density, compressive strength and water absorption tests.

iii) To perform scanning electron microscopy, Raman spectroscopy and thermogravimetric analyses on the materials studied.

iv) To correlate the macroscopic and microscopic properties of the materials studied.

v) To comparatively evaluate which material offers the best thermal performance.

vi) To provide inputs for strengthening and revising the ABNT and Mercosur standards.

1.2 RELEVANCE AND IMPACTS

The motivation for this work lies in the need to promote standard harmonization among Mercosur countries, focusing on the thermal suitability of wall materials. The research seeks to make a technical contribution to strengthening the ABNT NBR NM standards and aligning thermal performance criteria in the regional construction context.

The main topics that will contribute to scientific, technological and innovation development can be highlighted, namely:

i) Strengthening innovative research, especially regarding construction materials.

ii) Developing research in favor of sustainable development and the dissemination of innovative products and techniques for construction in Latin America.

iii) Contributing to the Sustainable Development Goals/2030 Agenda of the United Nations (UN), highlighting the potential contribution to the following goals: Good health and well-being (SDG 3); Affordable and clean energy (SDG 7); Decent work and economic growth (SDG 8); Industry, innovation and infrastructure (SDG 9); Sustainable cities and communities (SDG 11); Responsible consumption and production (SDG 12); Climate action (SDG 13); Life below water (SDG 14); Life on land (SDG 15); Partnerships for the goals (SDG 17).

1.3 STATEMENT ON THE USE OF ARTIFICIAL INTELLIGENCE

Generative artificial intelligence tools, such as ChatGPT-5.6 Luna and Claude Sonnet 5, were used as an auxiliary resource in specific stages of the research process, in accordance with UNESCO's (2021) recommendations on the ethics of Artificial Intelligence (AI). The use of AI was restricted to the following support functions: i) assisted reading and organization of experimental data; ii) support in the preliminary interpretation of analyses; iii) graphic adaptation; iv) proofreading.

1.4 STRUCTURE OF THE DISSERTATION

This dissertation is organized into eight chapters. Chapter 1 presents the introduction, with the background of the topic, the objectives, the relevance and impacts of the research and the statement on the use of artificial intelligence. Chapter 2 brings together the fundamentals of the thermal performance of wall systems and the energy efficiency of buildings, with emphasis on the thermal characteristics of construction materials. Chapter 3 discusses the standard prescriptions on thermal comfort in Brazil and Argentina and presents a comparative analysis of the two sets of standards. Chapter 4 describes the materials and methods, including the characterization of the cities of Juiz de Fora and Santa Fe, the ceramic and concrete blocks investigated and the stages of the experimental program. Chapter 5 presents and discusses the results of the macroscopic, scanning electron microscopy, Raman spectroscopy, thermogravimetric and thermal conductivity tests, first for the ceramic blocks and then for the concrete blocks, closing with an integrated analysis of the four materials. Chapter 6 presents the conclusions, the inputs for standard revision within Mercosur and recommendations for future work. Chapter 7 acknowledges the support and funding received for the research and, finally, Chapter 8 lists the references used.

2 THERMAL PERFORMANCE OF WALL SYSTEMS AND ENERGY EFFICIENCY OF BUILDINGS

2.1 INITIAL CONSIDERATIONS

Evaluating the thermal performance of wall systems and its relationship with the energy efficiency of buildings requires understanding an articulated set of concepts, properties and parameters that govern the thermal behavior of built environments.

The concept of thermal comfort refers to the desirable thermal conditions in buildings that influence occupants' well-being and performance. It is usually assessed through computer simulations, user questionnaires and indices such as effective temperature (Pereira *et al*., 2020; Cavalcanti, 2020), and it is closely related to the design's response to the microclimate (Suryo, 2019).

According to Pagnossin, Buriol and Graciolli (2001), thermal comfort is related to the feeling of satisfaction with the thermal environment and is influenced by physical factors, such as the heat exchange mechanisms (conduction, convection, radiation and evaporation) that promote energy gains or losses in the body. In addition, meteorological variables such as temperature, humidity, air movement and radiation also affect this perception, as do individual physiological and psychological aspects, which vary according to each person's thermal sensitivity and preference.

Energy efficiency consists of the rational use of energy to achieve a given result, that is, the relationship between the amount of energy used in an activity and that made available for it (Tigre, 2016); it also helps reduce consumption without compromising users' well-being (CBCS, 2015). In the construction sector, according to data from the Brazilian Council for Sustainable Construction (CBCS) (2015), energy efficiency in buildings was considered one of the areas with the greatest potential for large reductions in energy consumption.

In turn, one of the main objectives of seeking adequate thermal performance is to minimize the energy consumption needed to achieve the desired thermal comfort (Filho, 2023).

Thermal transmittance[1] is one of the essential properties of the building envelope and is decisive for evaluating its thermal performance (Cavalcanti, 2020).

[1] Thermal transmittance is defined as a measure of the rate of heat transfer through a material or building component (Cavalcanti, 2020).

The use of passive thermal conditioning techniques suited to the local climate helps improve the thermal performance of buildings (Suryo, 2019). This type of conditioning refers to the set of architectural strategies and solutions aimed at keeping the indoor environment thermally comfortable using only natural resources, without mechanical equipment (Bhamare, Rathod and Banerjee, 2019).

According to Bhamare, Rathod and Banerjee (2019), these strategies include cross ventilation, shading, proper solar orientation, the thermal inertia of materials and the use of water evaporation. By exploiting local climatic conditions and the characteristics of the building itself, the aim is to minimize the need for active air conditioning, promoting energy efficiency.

In this sense, Soliman *et al*. (2022) highlighted the essential role of construction materials as a means of achieving building energy efficiency, as well as their influence on the life cycle of buildings, emphasizing that, beyond a sustainable outcome, changes in material selection specifications and guidelines are needed.

Therefore, decisions made during the design stage have a significant impact on the thermal and energy performance of the building (Brígitte and Ruschel, 2016). In this sense, studying the thermal properties of construction materials is crucial to combining comfort and energy efficiency (Barbosa, Aguilar and Sales, 2021).

2.2 THERMAL CHARACTERISTICS OF CONSTRUCTION MATERIALS

The thermal properties of materials determine how heat is transferred through building elements. Characteristics such as thermal conductivity, diffusivity and capacity are decisive in ensuring the energy performance and thermal comfort of buildings (Santos, 2008; Barbosa, Aguilar and Sales, 2021).

This scenario shows that the careful selection of construction materials is essential to promote efficient energy use and, when combined with building technologies, has the potential to significantly reduce energy consumption, especially regarding the demand for mechanical heating and cooling of buildings (Kamal, 2015).

In construction, the envelope is a fundamental structure in the formation of a building (Filho, 2023). Therefore, understanding and analyzing the properties, especially of the envelope materials, is essential for planning energy-efficient buildings (Oliveira and Lunardi, 2018).

Gomes and Melo (2018) highlight that the building envelope, especially the wall system, plays an essential role in controlling heat flow into indoor spaces, and

deficiencies in external masonry can result in thermal discomfort due to excessive heat gain from outside. This importance is reinforced by Kumar et al. (2020), who point out that the envelope accounts for 50% to 60% of the total heat gain or loss in a building.

Reducing heat losses through the envelope, combined with an optimized configuration of materials and the proper application of insulation and thermal mass, contributes significantly to lowering the energy demand for heating and cooling (Qin *et al.*, 2021). This approach also results in mitigation of the carbon dioxide emissions associated with the building's thermal performance (Kamal, 2015).

According to Filho (2023), the law of heat conduction[2], or Fourier's law, states that the heat flux in a material is proportional to the temperature gradient along it, representing the material's tendency to reach thermal equilibrium, in which the energy received is transmitted between the particles that make up the solid body. Furthermore, thermal conductivity is a characteristic physical property of the material.

Kumar et al. (2020) emphasize that insulation of the building envelope is crucial for a comfortable indoor environment. They point out that insulation materials can be mainly categorized as conventional; state-of-the-art (the lowest thermal conductivity among the three types of insulation); and sustainable. Their purpose is to delay and minimize the maximum indoor temperature and reduce the risk of overheating during hot summer periods, as well as to help reduce heat losses from the indoor environment to the outside during winter, favoring the maintenance of thermal comfort and lowering energy consumption for heating.

Furthermore, the hygroscopic, acoustic and fire resistance properties of wall materials play a fundamental role in the overall performance of buildings. These characteristics are essential for controlling relative humidity in regions with high humidity levels, attenuating noise in sound-sensitive areas and reducing the spread of and damage caused by fires.

Insulation materials used in the construction industry include cork, cellulose, rock wool, sheep's wool, expanded polystyrene, perlite, coconut husk, cotton waste, bagasse, rice husk ash and textile ash residues (Ijjada and Nayaka, 2022). The careful selection of materials requires several tests to evaluate their mechanical, chemical and thermal properties, such as heat flow measurement, the hot-wire method for thermal

[2] Thermal conductivity is defined as the rate of energy transmission, in the form of heat, through a material over time. In the International System of Units, the unit for this physical quantity is the watt per meter per kelvin (W/m·K) (Filho, 2023).

conductivity, absorption tests, porosity, calorimetry and gravimetric analysis. These tests make it possible to verify the material's performance in terms of thermal conductivity, moisture retention and durability, ensuring an appropriate selection for its final application (Nasr *et al*., 2023).

3 STANDARD PRESCRIPTIONS ON THERMAL COMFORT

Although there are standards for Mercosur countries, this study focuses on the national standards applicable to each city studied, given their direct application in local building practices and in the legal requirements in force in each context, as well as the characteristics of the construction materials used in the case study.

3.1 BRAZILIAN STANDARDS

The Brazilian standard NBR 15575-1 (ABNT, 2024), whose first version came into force in 2013, emerged as a response to the need to define criteria and objectives for the performance of residential buildings in Brazil. In short, it establishes performance requirements for the in-use behavior of residential buildings and their systems, addressing essential aspects such as habitability (including thermal comfort), safety, functionality and sustainability.

Regarding thermal comfort, the standard establishes that the thermal performance of buildings must be evaluated based on the behavior of the external vertical wall systems, using two main methods: the simplified procedure and computer simulation, according to NBR 15575-1 (ABNT, 2024) (Figure 4).

Figure 4 – Thermal performance assessment methods.

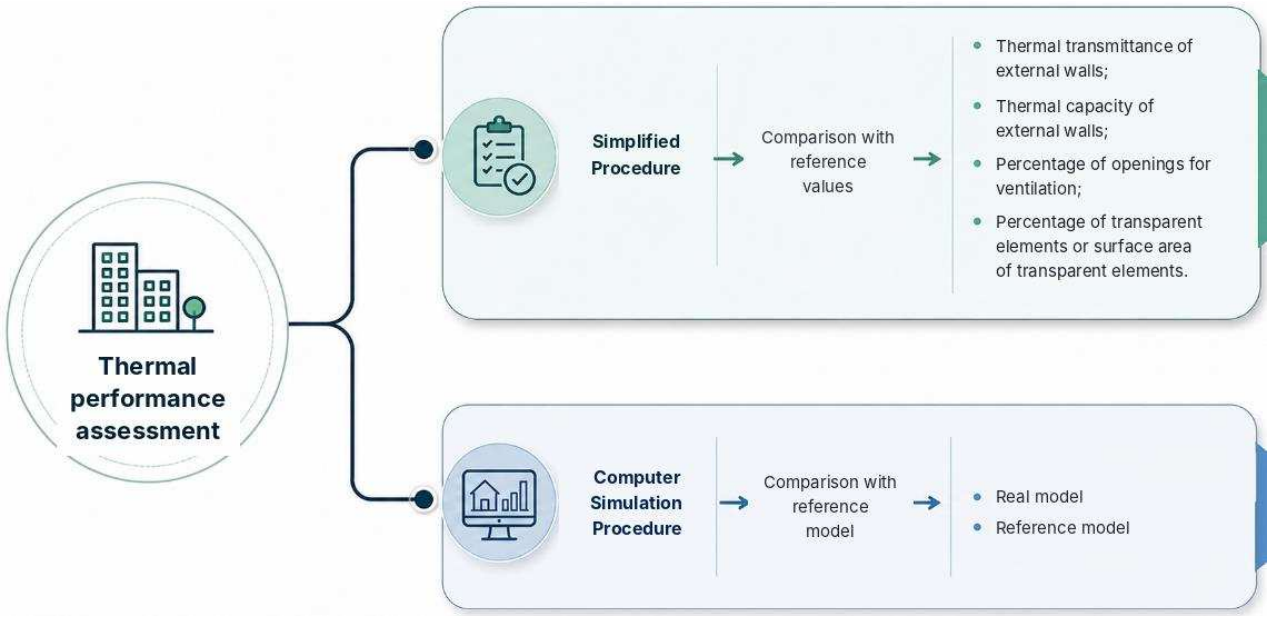

Source: Adapted (2026) from ABNT NBR 15575-4 (2021) and generated with ChatGPT-5.6 Luna (2026).

That said, one of the main objectives of the standard is to ensure that the indoor conditions of a building are able to provide thermal comfort to users in the different seasons of the year (ABNT, 2021). That is, in summer the indoor temperature should not exceed the outdoor temperature, while in winter the indoor temperature should be at least 3 °C higher than the outdoor temperature, ensuring thermal comfort for users (Guarda, Durante and Callejas, 2020; ABNT, 2021).

The Simplified Procedure evaluates the minimum thermal performance of the building by comparing it with reference values for the thermal transmittance of external walls, the thermal capacity of external walls, the percentage of openings for ventilation and the percentage of transparent elements or surface area of transparent elements, NBR 15575-4 (ABNT, 2021), according to the bioclimatic zone in which the building is located (Santos *et al*., 2015). The Computer Simulation Procedure, in turn, evaluates thermal performance at the minimum, intermediate and superior levels by comparison with a reference model, allowing design adjustments to ensure compliance with the established criteria (Sorgato *et al*., 2012).

For both types of thermal performance evaluation described in NBR 15575-4 (ABNT, 2021), a method for measuring the thermal properties of materials and building elements in Brazil must also be adopted.

In this context, the selection of materials and building systems must meet the thermal performance requirements established by NBR 15575-4 (ABNT, 2021), as they have a direct impact on achieving comfortable, efficient and sustainable environments for users that meet thermal and energy performance standards (Carneiro and Oliveira, 2020).

In parallel, in practice, since its implementation, NBR 15575-1 (ABNT, 2024) has driven changes in the Brazilian construction sector, mainly related to building envelopes. Studies show that small changes in the design and in the specification of façade materials can ensure minimum performance levels that meet the requirements of the standard without significantly changing the cost of the product (Bueno *et al*., 2019).

However, according to Nunes et al. (2021), despite the time elapsed and its wide dissemination, the standard is still not fully known and widespread, which highlights the need for actions to broaden understanding of its importance and ensure the implementation of its requirements in buildings. Thus, the constant evaluation and

improvement of the methods defined by the standard are essential for the progress of the sector and for improving the quality of construction in the country (Chvatal, 2014).

In turn, NBR 15220-3 (ABNT, 2024): Thermal performance of buildings - Part 3: Bioclimatic zoning by performance, one of the first standards to address the topic, focuses on establishing a Brazilian bioclimatic zoning for thermal performance analyses, applicable to residential buildings (single-family or multi-family) as well as to non-residential and non-industrial buildings.

NBR 15220-3 (ABNT, 2024) focuses on dividing the Brazilian territory into 8 bioclimatic zones (Figure 5), with recommendations of passive thermal conditioning strategies (Martins, Bittencourt and Krause, 2012).

Figure 5 – Map of Brazil with the 8 bioclimatic zones.

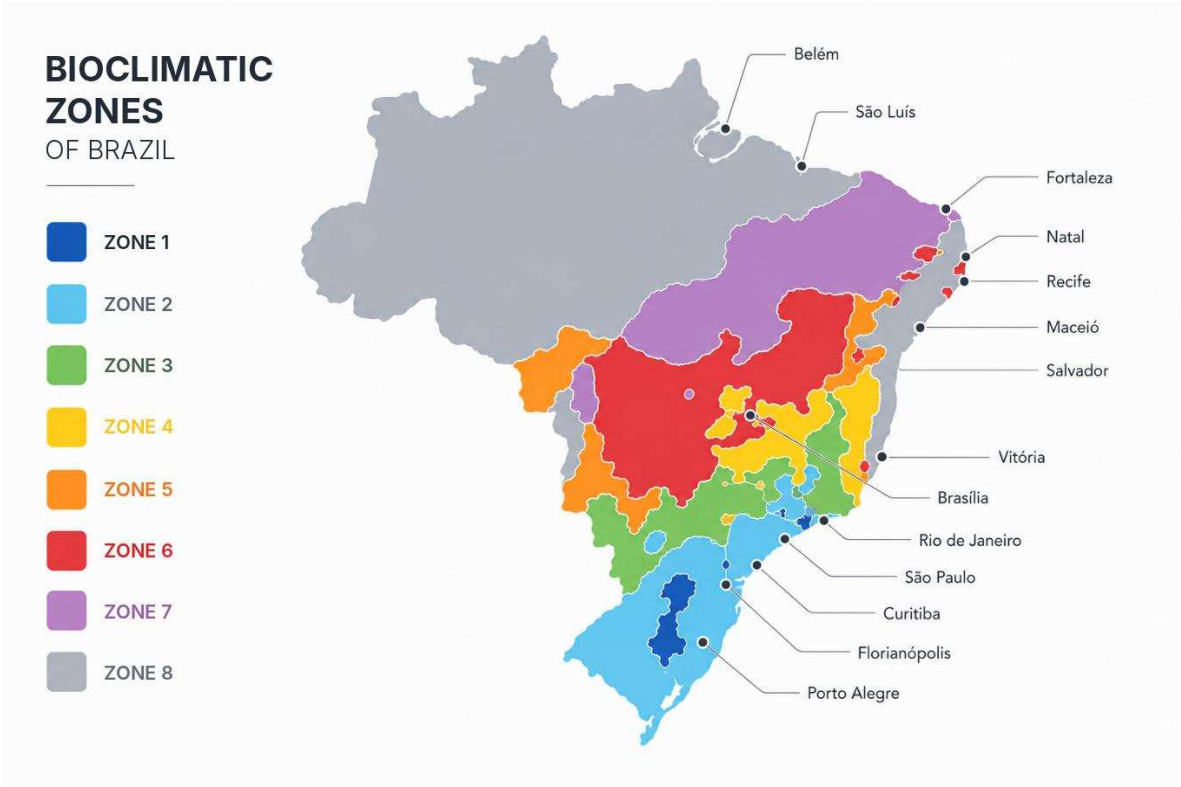

Source: Adapted (2026) from Lamberts (2016) and generated with ChatGPT-5.6 Luna (2026).

For each Brazilian bioclimatic zone, parameters such as the size of ventilation openings, shading of openings, external walls and roofs (type of external wall and type of roof) and passive thermal conditioning strategies are considered to ensure thermal comfort inside buildings, according to the specific climatic conditions of each region (Lamberts, 2016). The construction guidelines regarding the admissible thermal

transmittance, thermal lag and solar heat gain factor for external walls stand out (see Table 1).

Table 1 – Admissible thermal transmittance, thermal lag and solar heat gain factor for each type of external wall.

External walls		**Thermal transmittance – U** (W/m²·K)	**Thermal lag – φ** (Hours)	**Solar factor – FSo** (%)
Walls	Light	U ≤ 3.00	φ ≤ 4.3	FSo ≤ 5.0
	Light reflective	U ≤ 3.60	φ ≤ 4.3	FSo ≤ 4.0
	Heavy	U ≤ 2.20	φ ≤ 6.5	FSo ≤ 3.5

Source: Adapted (2026) from ABNT NBR 15220-3 (2024).

In addition, NBR 15220-2 (ABNT, 2024) provides guidance on the thermal properties of wall materials such as ceramics, plaster or bedding mortar and concrete (see Table 2), used in components such as blocks.

Table 2 – Thermal properties of materials.

Material	**ρ** (kg/m³)	**λ** (W/(m·K))	**c** (kJ/(kg·K))
Ceramic	1,600	0.90	0.92
Plaster or bedding mortar	2,000	1.15	1.00
Concrete	2,400	1.75	1.00

Source: Adapted (2026) from ABNT NBR 15220-2 (2024).

Table 2 presents reference values for characteristics such as density (ρ), thermal conductivity (λ) and specific heat (c), which directly influence the thermal behavior of building elements. Materials such as ceramics, mortar and concrete, commonly used in masonry and finishes, have different heat conduction and storage capacities, directly affecting indoor thermal comfort and the thermal inertia of the building.

In view of the above, it is concluded that the NBR 15575 and NBR 15220 standards are essential to guide the thermal performance of buildings, as they establish specific criteria according to the Brazilian bioclimatic zones.

3.2 ARGENTINE STANDARDS

The main objective of IRAM 11601 (IRAM, 2004), which deals with the thermal insulation of buildings, is to establish criteria, reference values and methods for determining the thermal properties of building components and elements, focusing on evaluating the thermal performance of the envelope according to regional bioclimatic conditions.

Furthermore, IRAM 11601 (IRAM, 2004) includes simplified methods for calculating non-homogeneous plane elements, applicable when the calculation of the structure is not covered by other standards, such as those dealing with thermal bridges. It is worth noting that these calculations do not take into account air infiltration through the elements, nor solar radiation on surfaces or through transparent elements (IRAM, 2004).

In addition to the calculations, IRAM 11601 (IRAM, 2004) also presents tables and annexes listing the thermal and hygrothermal properties of materials typically used in Argentine construction, from which Table 3 reproduces the density (ρ) and water vapor permeability (δ) of some finishes and masonry types, as well as methods for the simplified verification of thermal resistance, practical application guides and a bibliography that underpins the calculations (IRAM, 2004).

Table 3 – Properties of materials according to IRAM 11601.

MATERIAL	**DENSITY (ρ)** (kg/m³)	**WATER VAPOR PERMEABILITY (δ)** (g/m·h·kPa)
FINISHES		
Porcelain-type ceramic tile with cement mortar	1,900	$0.32 \cdot 10^{-2}$
Glazed tiles with cement mortar	1,700	$0.32 \cdot 10^{-2}$
Plastic and rubber	1,300	$0.08 \cdot 10^{-2}$
MASONRY		
Made of common solid bricks with mortar and without plaster	1,500	$8.0 \cdot 10^{-2}$
Made of load-bearing ceramic blocks with vertical holes, mortar bed and without plaster	850 to 1,200	$10.0 \cdot 10^{-2}$
Made of load-bearing ceramic blocks with horizontal holes, with mortar bed and without plaster	850 to 1,100	$13.0 \cdot 10^{-2}$

Source: Adapted (2026) from IRAM (2004).

Furthermore, IRAM 11605 (IRAM, 2002) focuses on ensuring minimum habitability conditions, promoting energy efficiency and thermal comfort. To this end, three comfort levels are defined: Level A (Recommended) offers the highest thermal comfort; Level B (Medium) provides intermediate thermal comfort; and Level C

(Minimum) ensures the minimum acceptable thermal comfort. The requirements established by the standard analyze winter and summer conditions separately (see Tables 4 and 5).

Table 4 – K_{maxadm} values for winter conditions in W/m²·K.

OUTDOOR TEMPERATURE (°C)	LEVEL A	LEVEL B	LEVEL C
	WALLS	WALLS	WALLS
-15	0.23	0.60	1.01
-14	0.23	0.60	1.04
-13	0.24	0.63	1.08
-12	0.25	0.65	1.11
-11	0.25	0.67	1.15
-10	0.26	0.69	1.19
-09	0.27	0.72	1.23
-08	0.28	0.74	1.28
-07	0.29	0.77	1.33
-06	0.30	0.80	1.39
-05	0.31	0.83	1.45
-04	0.32	0.87	1.52
-03	0.33	0.91	1.59
-02	0.35	0.95	1.67
-01	0.36	0.99	1.75
≥ 0	0.38	1.00	1.85

Source: Adapted (2026) from IRAM (2002).

Table 4 presents the maximum admissible thermal transmittance values (Kmaxadm) for walls at different outdoor temperatures during winter. The lower the K value, the greater the insulation and indoor thermal comfort.

Table 5 – Maximum thermal transmittance values for walls under summer conditions in W/m²·K.

BIOENVIRONMENTAL ZONE	LEVEL A	LEVEL B	LEVEL C
I and II	0.45	1.10	1.80
III and IV	0.50	1.25	2.00

Source: Adapted (2026) from IRAM (2002).

Table 5, in turn, establishes the maximum thermal transmittance values for walls in W/m²·K in summer, considering the bioenvironmental zones of Argentina (zones I and II and zones III and IV). The aim is to reduce heat gain, promoting thermal comfort and energy efficiency.

Finally, IRAM 11900 (IRAM, 2019) establishes a methodology for evaluating and rating the energy efficiency of buildings in Argentina, with the aim of standardizing criteria at the national level and facilitating the implementation of public policies aimed at energy saving. The rating is carried out through a performance label, which evaluates the building's energy consumption and classifies it on a letter scale from A to G, A being the most efficient level and G the least efficient.

3.3 COMPARATIVE ANALYSIS OF THE STANDARDS

In summary, the Argentine standards IRAM 11601 (IRAM, 2004), IRAM 11605 (IRAM, 2002) and IRAM 11900 (IRAM, 2019) and the Brazilian standards NBR 15575 (ABNT, 2024) and NBR 15220-3 (ABNT, 2024) diverge in the criteria and requirements related to the thermal performance of buildings (see Table 6). The Argentine standard requires lower thermal transmittance values for walls, with specific requirements for the heating coefficient and the thermal load, in addition to requirements for preventing condensation on walls and ceilings (Netto and Czajkowski, 2016), aspects not addressed in NBR 15575.

On the other hand, NBR 15575 (ABNT, 2024) is comprehensive in scope, regulating not only thermal performance but also aspects such as structural safety, acoustic performance and durability of buildings. In addition, the Brazilian standard allows alternative evaluation methods, such as computer simulation, while the Argentine regulations adopt direct criteria for materials and building systems (Netto; Czajkowski, 2016).

In view of the above, both sets of standards have potential for improvement, either through the adoption of more specific criteria in Brazil or through broader applicability and enforcement of the standards in Argentina, aiming at more efficient and comfortable buildings, as shown in Table 6.

Table 6 – Comparative summary of Brazilian and Argentine standards.

	Brazil	**Argentina**
Objective	To establish minimum performance criteria for buildings in several aspects, including thermal comfort.	To ensure the thermal insulation, comfort and energy efficiency of buildings, with a specific focus on thermal components.

Evaluation methods	Simplified Procedure and Computer Simulation (compared with a reference model).	Direct methods (K limit values), tables of thermal properties and simplified methods for non-homogeneous elements.
Thermal performance rating	Three levels: minimum, intermediate and superior. Evaluation based on bioclimatic zone.	Three levels: A (recommended), B (medium) and C (minimum), with distinctions between winter and summer.
Climatic zoning	8 bioclimatic zones defined by NBR 15220-3, with specific guidelines for each zone.	Bioenvironmental zones with specific tables for summer and winter, based on outdoor temperature.
Required thermal parameters	Thermal transmittance (U), thermal lag (φ), solar factor (FSo) and thermal properties of materials.	Maximum thermal transmittance (Kmaxadm), vapor permeability, density, among others.
Thermal comfort criteria	Indoor temperature should not be higher than outdoor temperature in summer and should be ≥ 3 °C higher in winter.	Maximum thermal transmittance according to outdoor temperatures; clear separation between winter and summer criteria.
Energy efficiency	Regulated indirectly by NBR 15575 and by the bioclimatic zoning.	IRAM 11900 defines a labeling and rating system for the energy efficiency of buildings.

Source: Prepared by the author (2026).

4 MATERIALS AND METHODS

4.1 INITIAL CONSIDERATIONS

This work was developed in partnership between the Centro de Investigación y Desarrollo para la Construcción y la Vivienda, CECOVI (Universidad Tecnológica Nacional – UTN Santa Fe) and the Graduate Program in Built Environment (Federal University of Juiz de Fora – UFJF) and investigates the influence of the thermal properties of construction materials used in non-load-bearing masonry (monolithic units), namely ceramic blocks and concrete blocks, with a view to the thermal performance of buildings and, consequently, the reduction of energy consumption (energy efficiency) (see Figure 6).

Figure 6 – Location of the cities of Juiz de Fora and Santa Fe.



Source: Map data Google (2025).

It should be noted that the cooperation between the academic institutions is a strategy of techno-scientific rapprochement, strengthening research networks at the Latin American level and fostering innovation in this topic and in other related fields of research. This cooperation will make it possible to consolidate a solid basis for developing policies, projects and practices that improve the habitability of the built environment in South America.

4.1.1 **The city of Juiz de Fora**

Juiz de Fora is a city located in the state of Minas Gerais, Brazil, and, according to the Brazilian Institute of Geography and Statistics (IBGE, 2022), in the last census in 2022 it had a total population of 540,756 inhabitants, with a population density of 376.64 inhab./km². The city lies at an altitude of between 700 m and 900 m above sea level, with a highly dissected relief of concave-convex hills and valleys, characteristic of the Paraíba do Sul Valley and the foothills of the Serra da Mantiqueira, and it is influenced by air masses with distinct characteristics (PMJF, 2018).

Regarding climate, Juiz de Fora has mean temperatures ranging from 12.8 °C to 28 °C and a high-altitude tropical climate with two well-defined seasons: a dry autumn/winter, with approximately 20% of the annual rainfall, and a rainy spring/summer, with about 80% of the annual rainfall (annual mean of 1,542.9 mm) (Ferreira *et al.*, 2023).

According to Oliveira et al. (2017), wind patterns are variable, depending mainly on the location of the measurement point and the time of day, with no predominant directions; winds of up to 3 km/h prevail in the lower part of the city (around 700 m) and up to 6 km/h at an altitude of 940 m.

Historically, Juiz de Fora emerged as a major industrial center in the late 19th and early 20th centuries, earning the nickname “Manchester Mineira” (Oliveira, 2020). Around 1703, the road known as Caminho Novo was built to connect the gold mining region to Rio de Janeiro. This route was intended to facilitate the transport of the extracted gold, allowing greater circulation of people through the region, which had previously been dense forest inhabited by a few Indigenous people of the Coroados and Puris tribes (PMJF, 2018).

The city's growth was driven by the construction of the União e Indústria road in 1861, which facilitated the transport of coffee production from the Zona da Mata and Paraíba Valley regions. Thus, two elements marked the main transformations of the city: coffee and industry (Bartolomeu, 2019).

Today, the city has a diversified economic base and a strong institutional profile, as it hosts the main campus of the Federal University of Juiz de Fora (UFJF) and four other private colleges.

4.1.2 **The city of Santa Fe**

Santa Fe is a city located in the province of Santa Fe, Argentina, and, according to the Instituto Nacional de Estadística y Censos (INDEC, 2022), in the last census in

2022 it had a total population of 572,265 inhabitants, with a population density of 192.2 inhab./km². The city lies at an altitude of 27 m above sea level and is strongly influenced by the Paraná River.

Regarding climate, Santa Fe has mean temperatures ranging from 8 °C to 31 °C (Servicio Meteorológico Nacional, 2024) and a humid subtropical climate with two rainy seasons, autumn and spring (mean annual rainfall between 900 mm and 1,000 mm) (Venturini, 2022).

As for wind patterns, according to Weather Spark (2018), during winter the mean hourly wind speed in Santa Fe increases from 13.8 km/h to 16.0 km/h over the season. The predominant wind direction varies between north, south and east.

Founded on November 15, 1573, by Juan de Garay, Santa Fe was first established in the region of Cayastá, known as “Santa Fe la Vieja”. Due to constant flooding and Indigenous attacks, the city was moved to its current location between 1650 and 1660 (Milano, 2011). It is considered the first port city of the Río de la Plata region, playing a crucial role in Spanish colonization and in the development of the Argentine interior.

In the 19th century, Santa Fe played a decisive role in the formation of the Argentine State and became a prominent political and legal center (Baretta, 2024).

In addition to its political role, Santa Fe stands out for its cultural and educational landscape. The city is home to renowned institutions such as the Universidad Nacional del Litoral, the Universidad Católica de Santa Fe and the Universidad Tecnológica Nacional – UTN Santa Fe (Wikipedia, 2025).

4.2 MATERIALS

This study evaluates the properties of monolithic units, namely ceramic blocks and concrete blocks, with the specimens collected according to the following criteria:

- Commercial availability: materials available from construction suppliers in the cities of Juiz de Fora and Santa Fe and widely used in the sector for non-load-bearing masonry in buildings, excluding structural elements or specific components for special finishes;
- Brazilian standardization: the blocks follow the most commonly used dimensional standard in the region and comply with current standards, with dimensions of 9 × 19 × 29 cm and 9 × 19 × 39 cm (width × height × length);

- Argentine standardization: the blocks follow the most commonly used dimensional standard in the region and comply with current standards, with dimensions of 8 × 17 × 32 cm and 9 × 19 × 39 cm (width × height × length);
- Total number of specimens per test and per type of material: six (6).

4.2.1 **Ceramic block**

One of the wall systems widely used in construction is ceramic block masonry. These blocks are produced from a clay body, shaped by extrusion to acquire a specific form and properties, and then fired at temperatures ranging from 800 °C to 1000 °C (Filho, 2023).

In this study, the Brazilian specimens were purchased from suppliers in the city of Juiz de Fora (MG). These materials are regulated by NBR 15270-1 (ABNT, 2023), which defines their specifications, including minimum mechanical strength, water absorption and geometry.

The Argentine ceramic blocks used in this research were purchased from suppliers in the city of Santa Fe, Argentina. These materials are regulated by specific IRAM standards, mainly IRAM 12566-1 and IRAM 12566-2 (IRAM, 2005), which establish the requirements for solid and hollow ceramic units, including compressive strength, physical characteristics and quality criteria.

4.2.2 **Concrete block**

The concrete block consists of a mixture of cement, coarse and fine aggregates and water. The aggregates may include gravel or crushed stone, natural and/or manufactured sand, or stone dust, and the resulting mix is a dry-consistency concrete (Filho, 2023).

In the case of Brazil, the concrete block used is a non-load-bearing block measuring 9 × 19 × 39 cm, purchased from suppliers in the city of Juiz de Fora (MG). These materials are regulated by NBR 6136 (ABNT, 2016), which establishes the acceptance requirements for plain hollow concrete blocks intended for masonry with or without a structural function, defining the ideal block types for each use. In addition, the standard regulates requirements for characteristic compressive strength, absorption and shrinkage.

The Argentine concrete block used is a non-load-bearing block measuring 9 × 19 × 39 cm, purchased from suppliers in the city of Santa Fe, Argentina. This material is regulated by the IRAM 11561 series (2018), which defines terminology, dimensional requirements, minimum mechanical strength, water absorption, test methods and sampling criteria, distinguishing between load-bearing and non-load-bearing blocks.

4.3 METHODS

The experimental procedure was carried out in two stages, with the aim of characterizing the materials and evaluating their thermal properties, namely: the evaluation of macroscopic properties (density, compressive strength and absorption) and of microscopic and thermal properties (scanning electron microscopy, Raman spectroscopy and thermogravimetric analysis), in addition to the determination of thermal conductivity (λ) and thermal resistance (R) by the heat flow meter method, in order to correlate the data with one another.

To facilitate the identification of the materials studied, the following nomenclature was adopted: BC refers to the ceramic block and BCC to the concrete block. The codes BR and AR indicate, respectively, the Brazilian and Argentine origin of the materials. Thus, BC BR refers to the Brazilian ceramic block, BC AR to the Argentine ceramic block, BCC BR to the Brazilian concrete block and BCC AR to the Argentine concrete block.

4.3.1 **Stage 1 - Evaluation of macroscopic properties**

Table 7 presents the tests performed and the relevant standards. It should be noted that 6 specimens were used for each test.

The tests on the Brazilian materials were carried out at the Civil Construction Materials Laboratory and the Strength of Materials Laboratory of the Federal University of Juiz de Fora, while those on the Argentine materials were carried out at the Centro de Investigación y Desarrollo para la Construcción y la Vivienda, CECOVI, of the Universidad Tecnológica Nacional (UTN Santa Fe).

Table 7 – Tests for the evaluation of the properties of each block and their respective standards.

TESTS PERFORMED	BC BR	BC AR	BCC BR	BCC AR
Apparent density	ABNT NBR 15270-2:2017	IRAM 12593:2004	ABNT NBR 12118:2013	IRAM 11561-4:2018
Water absorption				
Compressive strength		IRAM 12586:2004		

Source: Prepared by the author (2026).

4.3.2 **Stage 2 - Evaluation of microscopic and thermal properties**

For the thermal and microscopic studies of the specimens, one sample was used, consisting of block fragments or powdered material obtained by grinding, representative of the mean value obtained in the macroscopic tests, and the following analyses were performed:

a) **Scanning electron microscopy (SEM).** Scanning Electron Microscopy (SEM) was used to analyze the microstructure of the materials, allowing observation of the surface morphology, the distribution and shape of the pores, the presence of cracks and the arrangement of the constituent phases. This technique enables a qualitative evaluation of the microstructural characteristics of the materials, contributing to the understanding of their physical and mechanical behavior. The analyses were performed on samples of ceramic blocks and concrete blocks using a Hitachi TM3000 Tabletop Microscope at the Center for Spectroscopy and Molecular Structure (NEEM) of the UFJF Department of Chemistry. Images were obtained at magnifications of 50x, 250x, 500x, 1,000x and 2,000x.

   The interpretation of the results was based exclusively on the morphological evidence observed in the micrographs, considering aspects such as porosity, matrix compaction, presence of discontinuities and surface characteristics of the materials. The analyses presented are descriptive and were used to compare the microstructural differences between the materials studied. Magnification calibration and general operating procedures followed the recommendations of ISO 16700 (ISO, 2016), and the terminology used is in accordance with ISO 22493 (ISO, 2014).

b) **Raman spectroscopy.** Raman spectroscopy was used to evaluate the chemical and mineralogical structure of the materials, making it possible to identify compounds, crystalline phases and molecular groups present in the samples from their characteristic vibrations. This technique enables the characterization

of the constituents of the materials and the analysis of possible compositional differences between the samples studied. The analyses were performed on samples of ceramic blocks and concrete blocks using a Bruker Multiram spectrometer at the Center for Spectroscopy and Molecular Structure (NEEM) of the UFJF Department of Chemistry, operating with an Nd:YAG laser (1064 nm) and a spectral range of 4000 to 50 cm^{-1}. The interpretation of the results was based on the identification of the characteristic Raman bands of the compounds present in the materials and on the comparison of the relative intensity of the observed peaks. The spectra were normalized to the band at around 145–148 cm^{-1}, associated with the anatase phase (TiO_2), allowing compositional variations between samples to be compared. In this way, it was possible to evaluate the degree of chemical and mineralogical homogeneity of the materials studied. Wavenumber axis calibration and spectrometer performance verification followed the guidelines of ASTM E1840 (ASTM, 2022) and ASTM E2529 (ASTM, 2016).

c) **Thermogravimetry.** Thermogravimetric analysis (TGA), with simultaneous recording of differential thermal analysis (DTA), was used to evaluate the mass change of the materials as a function of increasing temperature, allowing their thermal stability and thermal decomposition events to be analyzed. This test makes it possible to identify mass losses associated with water evaporation, decomposition of organic compounds and physicochemical transformations of the materials. The analyses were performed on samples of ceramic blocks and concrete blocks using a DTG-60 Simultaneous DTA-TG Apparatus at the Center for Spectroscopy and Molecular Structure (NEEM) of the UFJF Department of Chemistry. During the test, the samples were subjected to controlled heating under a nitrogen (N_2) atmosphere over a temperature range of 25 °C to 600 °C, at a heating rate of 10 °C/min.

   The interpretation of the results was based on the mass change as a function of temperature, considering both the magnitude of the mass losses and the temperature ranges in which they occurred. In this way, it was possible to identify differences in the thermal behavior of the materials related to their chemical composition and manufacturing processes, allowing the degree of thermal stability under heating to be evaluated. The test was conducted according to the general principles of ASTM E1131 (ASTM, 2020) and ISO 11358-1 (ISO, 2022), with temperature calibration according to ASTM E967 (ASTM, 2018).

d) **Thermal conductivity**. Thermal conductivity (λ) and thermal resistance (R) were determined under steady-state conditions by the heat flow meter (HFM) method at the Conductivity Laboratory of the Centro de Investigación y Desarrollo para la Construcción y la Vivienda (CECOVI), UTN Santa Fe, using an HFM 446 Lambda Medium instrument (Netzsch), in accordance with IRAM 1860 (IRAM, 2002). To ensure the accuracy and metrological traceability of the results, the instrument is periodically calibrated with a certified fiberglass reference board (NIST SRM 1450D). The test is based on Fourier's law for one-dimensional steady-state heat conduction, with thermal conductivity obtained from Equation 1 and thermal resistance from Equation 2 (Barrientos Santini; Carrara, 2026).

$$\lambda = \frac{Q}{A} \cdot \frac{L}{\Delta T} \quad (1)$$

$$R = \frac{L}{\lambda} \quad (2)$$

Where: λ is the thermal conductivity (W/m·K); Q/A is the mean heat flux per unit area (W/m²), measured continuously by the instrument's transducers; L is the specimen thickness (m); ΔT is the temperature difference between the upper and lower plates in contact with the specimen (K); and R is the thermal resistance (m²·K/W).

Since the original dimensions of the blocks exceeded the capacity of the test chamber, the hollow blocks were cut in half and one of the sections was tested. To evaluate the concrete matrix without the effect of the air cells, flat slabs were also obtained from the Argentine concrete blocks by mechanically removing the internal webs, and flat concrete slabs of Brazilian origin were tested. Before testing, the specimens were oven-dried at 80 ± 2 °C to constant mass (variation of less than 0.2% between two successive weighings at a 24 h interval) and then stabilized in a desiccator with silica gel for 30 minutes. The plan dimensions were obtained as the mean of six measurements (three on each face), and the thickness was measured automatically by the instrument at a contact pressure of 2 kPa. The tests were conducted at a mean temperature of approximately 20 °C (instrument plates at about 10 °C and 30 °C), the reference condition of IRAM 11601 (IRAM, 2004), which made it possible to compare the results with the values tabulated in this standard and in ABNT NBR 15220-2 (ABNT, 2024).

Finally, a comparative analysis of the test results and their correlation was carried out, as shown in Figure 7.

Figure 7 – Methodological flowchart.

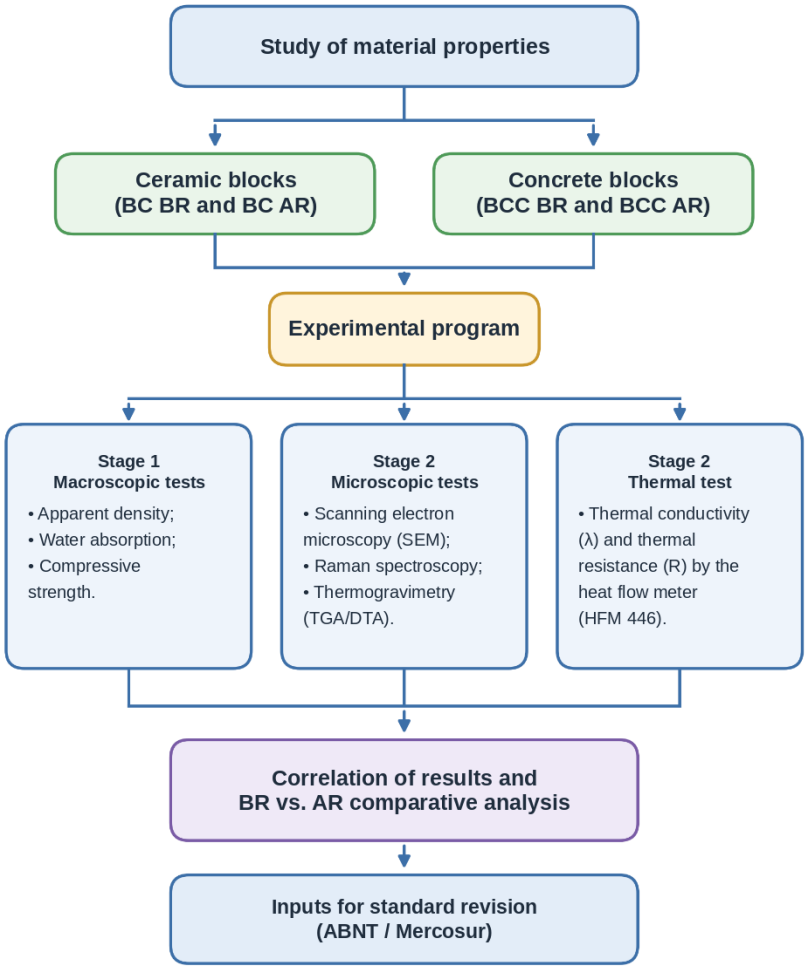

Source: Prepared by the author (2026) with the aid of ChatGPT-5.6 Luna (2026).

5 RESULTS AND ANALYSES

5.1 CERAMIC BLOCKS

5.1.1 **Macroscopic tests**

In order to characterize the blocks, tests were carried out according to current standards to determine the apparent density (ρap), water absorption (AA) and compressive strength (fbk), whose mean results are presented together with their respective coefficients of variation (CV) in Table 8. This simplified statistical procedure is used when the variability of several samples relative to their mean value is to be compared; the sample is accepted if the CV is below 25%.

Table 8 – Mean results of the tests performed on the BC.

SAMPLE	DIMENSIONS (cm)	ρ_{ap} (kg/m³)	AA (%)	f_{bk} (MPa)
BC BR	9.09 × 18.69 × 28.2 (CV = 0.31%)	2,072.94 (CV = 2.87%)	22.67 (CV = 12.26%)	1.44 (CV = 2.1%)
BC AR	8.15 × 17.70 × 32.17 (CV = 0.28%)	1,718 (CV = 0.85%)	15 (CV = 0.67%)	1.2 (CV = 16.54%)

Source: Prepared by the author (2026).

From Table 8, it can be observed that:

i) BC BR

The Brazilian ceramic blocks showed a mean apparent density of 2,072.94 kg/m³ (CV = 2.87%), a water absorption of 22.67% (CV = 12.26%) and a mean compressive strength of 1.44 MPa (CV = 2.1%), slightly below the minimum of 1.5 MPa required by NBR 15270-1 (ABNT, 2023) for non-load-bearing blocks.

ii) BC AR

The Argentine ceramic blocks, in turn, showed a mean apparent density of 1,718 kg/m³ (CV = 0.85%), lower than that observed for the Brazilian material. The mean water absorption was 15% (CV = 0.67%), also lower than that of the Brazilian material. The mean compressive strength was 1.2 MPa (CV = 16.54%), close to that obtained for the Brazilian blocks, although slightly lower. Taking the same minimum of 1.5 MPa of NBR 15270-1 (ABNT, 2023) as a reference, BC AR would also fall below this value; however, as it is an Argentine material, its compliance should be checked against the

minimum compressive strength requirement of IRAM 12566-2 (IRAM, 2005), which establishes a minimum characteristic compressive strength of 1.5 MPa for non-load-bearing ceramic blocks and 4.0 MPa for load-bearing ones. With a mean of 1.2 MPa, BC AR would also fall below the minimum requirement of this standard.

iii) BC BR vs. BC AR

Comparing the two materials, it can be observed that the Brazilian ceramic blocks had a higher apparent density than the Argentine ones, which suggests a denser internal structure and a lower relative pore volume in the Brazilian material. This greater compactness, however, did not translate into lower water absorption; on the contrary, the Brazilian blocks absorbed significantly more water (22.67%) than the Argentine ones (15%).

This apparently contradictory behavior can be explained by the fact that absorption depends not only on the total pore volume but mainly on the distribution and connectivity of the pores within the ceramic matrix. As for compressive strength, the two materials showed similar mechanical performance, with the Brazilian blocks (1.44 MPa) slightly stronger than the Argentine ones (1.2 MPa). Welch's t-test ($n = 6$ per material) indicated that this difference is statistically significant at the 5% level ($t \approx 2.9$; $df \approx 5$; $p \approx 0.03$), although small in absolute terms and associated with the high scatter of the BC AR results (CV = 16.54%). Both materials show the low load-bearing capacity characteristic of non-load-bearing ceramic blocks, resulting from the porosity inherent to the clay firing process.

5.1.2 **Scanning Electron Microscopy (SEM)**

The microstructural analysis was performed by Scanning Electron Microscopy (SEM) at magnifications of 50x, 250x, 500x, 1,000x and 2,000x (see Figures 8 and 9). The descriptions are based on the visual characteristics observed in the images obtained.

i) BC BR

Figure 8 presents the micrographs of BC BR at magnifications from 50x to 2,000x.

Figure 8 – Magnifications of 50x, 250x, 500x, 1,000x and 2,000x of BC BR.

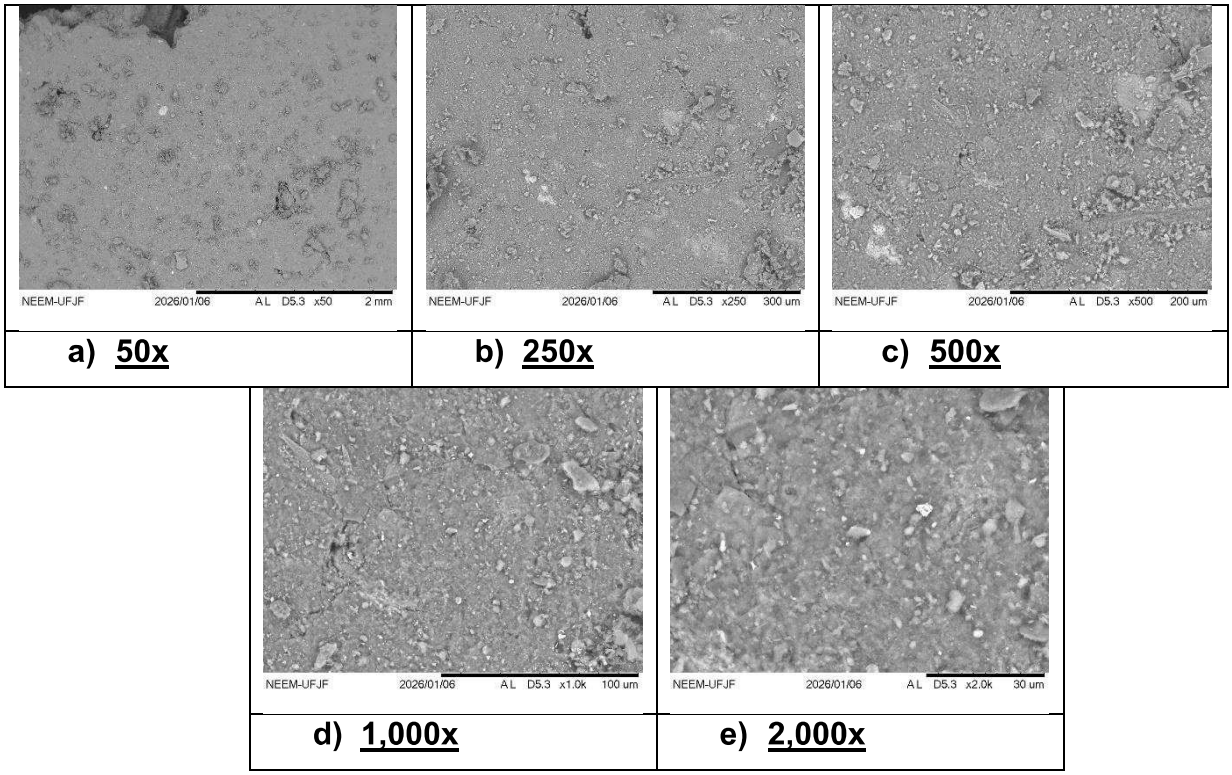

Source: Images obtained with the Hitachi TM3000 Tabletop Microscope at the Center for Spectroscopy and Molecular Structure (NEEM) of the UFJF Department of Chemistry (2026).

At 50x magnification, the ceramic block shows an irregular texture, with regions of different shades and possible variations in relief, which may indicate a non-uniform composition. In addition, isolated discontinuities and irregularities distributed over the surface are identified.

At 250x magnification, the structure reveals particles of varying sizes and small visible pores distributed over the surface.

At 500x magnification, the irregularly shaped particles, known as angular grains, become more evident, as do the spaces between them. At this magnification, the contact points between these particles are few, which suggests that they did not fully bond during firing.

This evidence therefore relates to a characteristic found in this type of material, known as incomplete particle consolidation, which contributes to the higher porosity and water absorption of the material.

At 1,000x magnification, the structure shows greater heterogeneity, with smoother regions and areas of angular grains. Small voids are also observed, which may be related to the release of gases during firing.

At the maximum magnification analyzed, 2,000x, agglomerates of particles with irregularly and heterogeneously distributed voids are observed, as seen previously. This confirms the low degree of densification of the material at this scale.

ii) BC AR

Figure 9 presents the micrographs of BC AR at magnifications from 50x to 2,000x.

Figure 9 – Magnifications of 50x, 250x, 500x, 1,000x and 2,000x of BC AR.

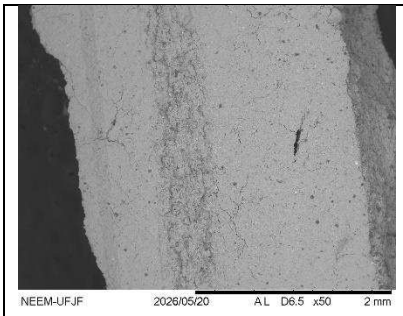

a) **50x**

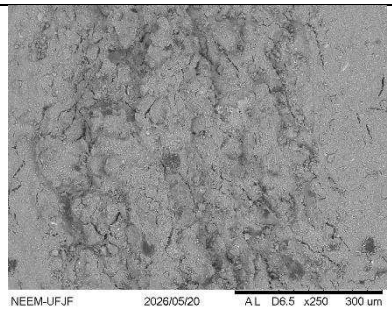

b) **250x**

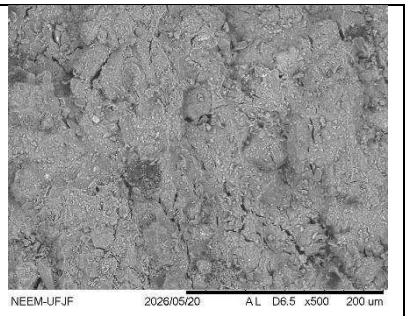

c) **500x**

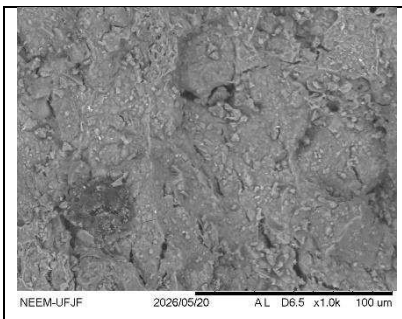

d) **1,000x**

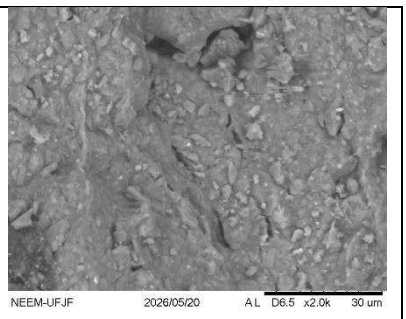

e) **2,000x**

Source: Images obtained with the Hitachi TM3000 Tabletop Microscope at the Center for Spectroscopy and Molecular Structure (NEEM) of the UFJF Department of Chemistry (2026).

At 50x magnification, the ceramic block shows a heterogeneous structure, with variations in density and relief, as well as irregularly distributed pores and elongated voids.

At 250x magnification, the microstructure reveals a matrix with an irregular surface, with particles of irregular and varied shapes, small visible cracks and regions with bands of different densities.

At 500x magnification, the particle boundaries become more evident, with angular shapes and few contact points. This suggests that the particles did not fully bond during firing.

At 1,000x magnification, the structure shows a heterogeneous area composed of more compact regions and regions with a rough texture. The particles have irregular shapes, with small voids distributed between the clusters. This analysis suggests that firing occurred at a moderate temperature, without fully densifying the material (Cultrone *et al.*, 2004).

At the maximum magnification analyzed, 2,000x, fine particles organized in irregular agglomerates are observed, with poorly bonded interfaces and heterogeneously distributed pores.

iii) BC BR vs. BC AR

Table 9 summarizes the correlation between the macroscopic properties and the SEM observations of the ceramic blocks.

Table 9 – Summary of the analysis of macroscopic vs. SEM results for BC BR vs. BC AR.

	Properties	**SEM**
BC BR	ρ_{ap} = 2,072.94 kg/m³ AA = 22.67% f_{bk} = 1.44 MPa	Porous structure with poorly bonded particles; Open and interconnected pores; Absence of complete fusion (bonding) between particles.
BC AR	ρ_{ap} = 1,718 kg/m³ AA = 15% f_{bk} =1.2 MPa	Heterogeneous structure with large voids; Poorly bonded particles; Low degree of densification; Absence of fusion between grains.

Source: Prepared by the author (2026).

The comparative analysis of the ceramic blocks reveals an apparently contradictory behavior between apparent density and water absorption: BC BR, despite having a higher apparent density (2,072.94 kg/m³) than BC AR (1,718 kg/m³), also showed higher water absorption (22.67% vs. 15%). This relationship indicates that apparent density and water absorption are governed by different microstructural

variables. While apparent density reflects the relationship between mass and total volume (solids and voids), water absorption is more directly associated with the connectivity of the pore network. The SEM images are consistent with this interpretation, suggesting for BC BR a structure with open and possibly interconnected pores, which favors capillary percolation of water even in a matrix of higher apparent density (Cultrone *et al*., 2004; Coletti *et al*., 2016).

From a microstructural point of view, both ceramic blocks showed evidence of incomplete particle consolidation, characterized by angular grain boundaries, few contact points between particles and the absence of complete fusion (bonding) between grains, indicating firing at a temperature or soaking time insufficient to achieve full densification of the clay matrix.

However, a relevant difference was observed regarding the homogeneity of the microstructure: while BC BR, although also heterogeneous, showed a relatively more uniform porosity pattern across the magnifications analyzed, BC AR revealed the coexistence of more compact regions with areas of rough texture and elongated voids, suggesting non-uniform firing throughout the ceramic body. This microstructural heterogeneity is partly consistent with the macroscopic data, since BC AR showed a considerably higher coefficient of variation in compressive strength (16.54%) than BC BR (2.1%), reinforcing the hypothesis of greater variability in the firing process and/or in the raw material used to manufacture the Argentine block, even though the CVs of ρap (0.85%) and AA (0.67%) for this material were low.

The low compressive strength values obtained for both blocks (1.44 MPa for BC BR and 1.2 MPa for BC AR) are consistent with the insufficient degree of densification identified by SEM. In porous ceramic materials, mechanical strength is strongly influenced by the amount, morphology and connectivity of pores, which act as stress concentrators and reduce the effective load-bearing area of the material's cross-section.

In this sense, although the two blocks show measurable physical differences, both share the same performance-limiting mechanism: the absence of complete sintering between the clay particles, consistently evidenced at the different magnifications analyzed. This finding suggests that, regardless of the origin of the material, the main factor determining the mechanical performance and potential durability of the blocks evaluated is associated with the quality of the firing process, and not solely with apparent density or raw material composition.

5.1.3 **Raman Spectroscopy**

The Raman spectra obtained for the ceramic blocks are presented below, first for each block and then comparatively.

i) BC BR

The Raman spectra of the ceramic blocks, normalized to the band at 148 cm^{-1}, corresponding to anatase (TiO_2), show that the samples analyzed have similar compositions, with minor variations in most of the identified peaks (except for the quartz band, discussed below), indicating low mineralogical variability among the samples (see Figure 10).

Figure 10 – Raman spectra of BC BR normalized to the 148 cm^{-1} band.

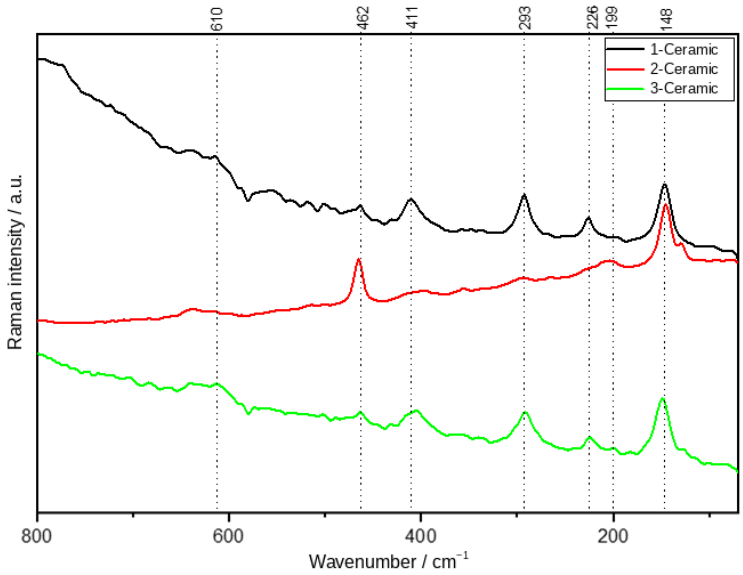

Source: Spectra obtained with the Bruker Multiram spectrometer at the Center for Spectroscopy and Molecular Structure (NEEM) of the UFJF Department of Chemistry, operating with an Nd:YAG laser (1064 nm) (2026).

The bands identified in the ceramic block samples are listed in Table 10.

Table 10 – Assignment of the Raman bands observed in the spectra of the BC BR samples investigated.

v / cm^{-1}	Assignment
148	**δ(O-Ti-O)**: Anatase
199	**Eg mode: Anatase**
226	**δ(Fe-O)**: Hematite
293	**δ(Fe-O)**: Hematite

411	**ν_s(Fe-O)**: Hematite
462	**ν_s(Si-O-Si)**: Quartz
610	**ν_{as}(Fe-O)**: Hematite

Source: Assignments made by the Center for Spectroscopy and Molecular Structure (NEEM) of the UFJF Department of Chemistry (2026).

The three BC BR samples show similar spectral profiles, with a predominance of bands assigned to hematite, the phase responsible for the reddish color of the materials, identified by the peaks at 226, 293, 411 and 610 cm^{-1}, in addition to the presence of quartz, identified at 462 cm^{-1}, and anatase, identified at 148 and 199 cm^{-1}. Sample 2-Ceramic, although it also contains hematite, stands out for the high intensity of the band at 462 cm^{-1}, suggesting a higher relative quartz content than the others.

The absence, in all samples, of bands associated with minerals containing water in their structure or with carbonate compounds reinforces that the material analyzed was chemically and mineralogically stabilized by the firing process.

In the range between 350 and 500 cm^{-1}, the vibrations associated with silicon–oxygen bonds, characteristic of quartz, stand out.

In the region between 600 and 800 cm^{-1}, contributions assigned to hematite (610 cm^{-1}) and possibly to aluminosilicates are observed, indicating thermal transformations consolidated during the firing process. This set of spectral evidence reinforces the interpretation of a material with high crystallinity and high thermal stability, indicating that firing was sufficient to chemically and mineralogically stabilize the phases present, but not to achieve the full densification of the matrix observed by SEM (see Table 11).

Table 11 – Interpretation of the BC BR band assignments.

Range (cm^{-1})	**Associated phase**	**Interpretation**
100–200	Crystal lattice / Anatase	-Low-frequency crystal lattice vibrations
200–300	Hematite	-Mineral formed during firing, responsible for the reddish color of the block
350–500	Si-O-Si / Quartz	-Stable silicate structures remaining from the original clay
462–464	Quartz	-Intense and characteristic peak; -Indicates the presence of silicate minerals with high thermal stability after firing.

600–800	Hematite and Aluminosilicates	-Thermal transformations consolidated during firing; -Indicates chemical and mineralogical stabilization of the phases by firing, without full densification (see SEM).

Source: Prepared by the author (2026).

ii) BC AR

The Raman spectrum of the ceramic block, normalized to the band at 145 cm^{-1}, corresponding to the anatase phase (TiO_2), reveals the predominant presence of three minerals: anatase, quartz and hematite (Figure 11).

Figure 11 – Raman spectrum of BC AR normalized to the 145 cm^{-1} band.

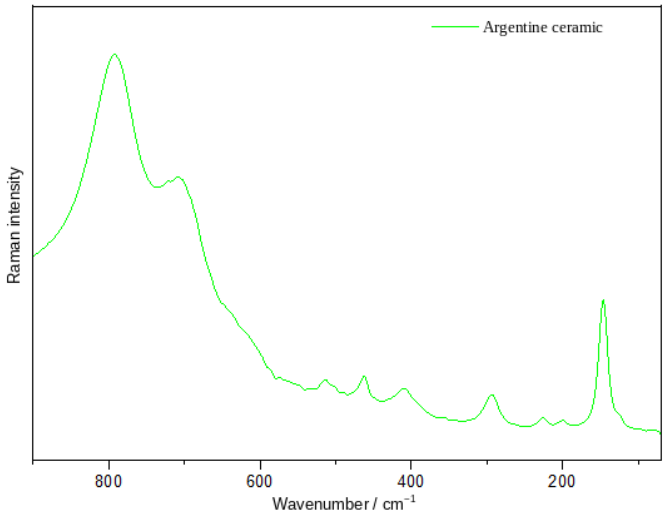

Source: Spectrum obtained with the Bruker Multiram spectrometer at the Center for Spectroscopy and Molecular Structure (NEEM) of the UFJF Department of Chemistry, operating with an Nd:YAG laser (1064 nm) (2026).

The bands assigned for the ceramic block investigated are presented in Table 12.

Table 12 – Assignment of the Raman bands observed in the spectra of the BC AR sample investigated.

v / cm^{-1}	Assignment
128	E mode: Quartz
145	E_g mode: Anatase
197	E_g mode: Anatase
293	E_g mode: Hematite
403	vs(Fe-O): Hematite / δ(Ti-O-Ti): Anatase
462	v_s(Si-O-Si): Quartz
514	A_{1g}+B_{1g} mode: Anatase

610	ν_{as}(Fe-O): Hematite
640	ν_{as}(Ti-O): Anatase

Source: Assignments made by the Center for Spectroscopy and Molecular Structure (NEEM) of the UFJF Department of Chemistry (2026).

The sample shows an intense, dominant peak in the 145 cm^{-1} region, which suggests a relevant presence of anatase in this material, bearing in mind that this phase has a high Raman scattering intensity and may stand out even at low contents. In addition to this main peak, bands at 197, 514 and 640 cm^{-1} are also observed and are likewise assigned to the anatase phase.

The bands identified at approximately 293, 403 and 610 cm^{-1} are consistent with characteristic vibrations of hematite, a mineral associated with the reddish color of fired ceramic materials. The band at around 462 cm^{-1} is assigned to quartz, indicating the presence of minerals remaining from the original clay used to manufacture the block.

Between 514 and 640 cm^{-1}, the signals reinforce the presence of anatase and hematite as thermally stable phases. The peaks observed are narrow and relatively well defined, characteristic of a material with an ordered crystal structure, the result of firing sufficient to chemically and mineralogically stabilize the phases, but not to achieve the complete sintering observed by SEM (see Table 13).

Table 13 – Interpretation of the BC AR band assignments.

Range (cm^{-1})	**Associated phase**	**Interpretation**
128–197	Quartz and Anatase	-Crystal lattice vibrations; anatase dominates the spectrum in this region, suggesting its relevant presence in the material.
293–403	Hematite and Anatase	-Crystalline metal oxides formed during firing; -Hematite is responsible for the reddish color of the block.
462	Quartz	-Characteristic quartz peak; -Indicates the presence of stable silicate minerals remaining from the original clay.
514–640	Anatase and Hematite	-Thermally stable phases consolidated by the firing process; -Reinforces the presence of anatase in the material.

Source: Prepared by the author (2026).

iii) BC BR vs. BC AR

Table 14 summarizes the correlation between the macroscopic properties and the Raman spectroscopy results of the ceramic blocks.

Table 14 – Summary of the analysis of macroscopic vs. Raman results for BC BR vs. BC AR.

	Properties	**RAMAN**
BC BR	ρ_{ap} = 2,072.94 kg/m³ AA = 22.67% f_{bk}= 1.44 MPa	Stable minerals (hematite, quartz, anatase); Well-defined crystal structure; Absence of hydrated compounds; Similar mineralogical composition among samples.
BC AR	ρ_{ap} = 1,718 kg/m³ AA = 15% f_{bk}= 1.2 MPa	Predominance of quartz, hematite and anatase; Crystalline mineralogical structure stabilized by firing; Absence of hydrated and carbonate phases; Predominantly crystalline and thermally stable material.

Source: Prepared by the author (2026).

The Raman spectroscopy analysis revealed qualitatively similar mineralogical profiles for BC BR and BC AR, both characterized by the predominance of the hematite, quartz and anatase phases, with characteristic bands at around 226–610 cm^{-1} (hematite), 462 cm^{-1} (quartz) and 145–199 cm^{-1} (anatase). In both materials, no bands associated with hydrated or carbonate compounds were observed, indicating that the firing process was sufficient to chemically and mineralogically stabilize the crystalline phases present in the clay raw material. This result indicates that the two ceramic blocks have qualitatively similar mineral phases; the differences lie mainly in the relative proportion of these phases, such as the higher relative quartz content in one of the BC BR samples and the higher anatase intensity in BC AR, reflecting the type of clay and the mix composition used in each country.

Both spectra showed narrow, well-defined peaks, a characteristic associated with ordered crystal structures resulting from firing processes sufficient for the chemical and mineralogical stabilization of the phases, although not for the full densification of the matrix observed by SEM. In BC AR, the higher relative intensity of the band at 145 cm^{-1}, associated with anatase, stands out, suggesting a slightly higher relative content of this phase than in BC BR, although in both materials hematite is the phase responsible for the reddish color characteristic of fired structural ceramics.

The presence of crystalline metal oxides (hematite and anatase) and quartz in both samples reinforces that, from a chemical-mineralogical standpoint, both blocks

reached a satisfactory degree of thermal transformation during firing, even though the physical consolidation between particles remained incomplete in both cases.

The convergence of the Raman results for BC BR and BC AR suggests that mineralogical composition alone does not explain the differences in physical and mechanical performance observed between the two materials. While BC BR showed higher water absorption (22.67%) and higher compressive strength (1.44 MPa) than BC AR (15% and 1.2 MPa, respectively), both exhibited compatible Raman profiles, with similar crystalline phases and equivalent mineralogical stabilization. Nevertheless, the Raman results suggest that the type of clay and the mix composition may influence the porosity of the blocks through minerals with low reactivity during firing, such as quartz, which hinder bonding between particles. However, this effect is attenuated by firing, which stabilizes the crystalline phases in both materials, so that the differences in performance manifest mainly in the shape, distribution and connectivity of the pores observed by SEM.

5.1.4 **Thermogravimetry**

The thermogravimetric curves obtained for the ceramic blocks are presented below, first for each block and then comparatively.

i) BC BR

Thermogravimetric analysis makes it possible to evaluate how the manufacturing process of each block's materials influences their behavior when subjected to heat (see Figure 12).

From Figure 12, it can be observed that:

a) 25 °C to 100 °C: A small mass loss is observed, which can be associated with the evaporation of water present on the surface and in the pores of the material. The low intensity of this event suggests that the ceramic block sample had a low moisture content.
b) 100 °C to 250 °C: The behavior is thermally stable, with no significant mass losses, indicating that no compounds are decomposing or releasing gases in this temperature range.
c) 250 °C to 450 °C: No significant thermal events were observed, indicating that the main transformations of the clay minerals had occurred previously during industrial firing.

d) 450 °C to 575 °C: The DTA curve shows a tendency to level off near its maximum.
e) 575 °C to 600 °C: Only a slight mass change was observed, indicating high thermal stability of the material.

Figure 12 – TGA and DTA curves of BC BR.

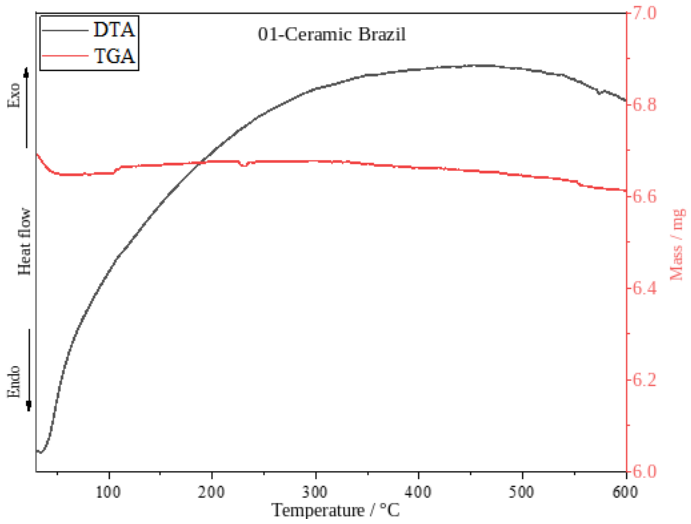

Source: Graph obtained from the test on the DTG-60 Simultaneous DTA-TG Apparatus at the Center for Spectroscopy and Molecular Structure (NEEM) of the UFJF Department of Chemistry (2026).

Thus, the Brazilian ceramic block showed a small mass loss throughout heating between 25 °C and 600 °C, demonstrating that the material is thermally stable. The absence of significant losses at higher temperatures indicates that industrial firing was sufficient to transform and chemically and mineralogically stabilize the minerals present in the clay, since the material did not undergo relevant transformations when heated, even though firing did not achieve the complete sintering observed by SEM (item 5.1.2).

ii) BC AR

Thermogravimetric analysis was also performed on the Argentine ceramic blocks (see Figure 13).

From Figure 13, it can be observed that:

a) 25 °C to 150 °C: A slight change in sample mass is observed, associated with the removal of water present on the surface and in the pores of the material.

b) 150 °C to 300 °C: The thermogravimetric curve remains stable, showing no significant thermal decomposition events.
c) 300 °C to 450 °C: Only a slight reduction in mass is observed, with no significant changes in the DTA curve, which is still rising in this region.
d) 450 °C to 600 °C: The small mass loss continues, with no abrupt events.

Figure 13 – TGA and DTA curves of BC AR.

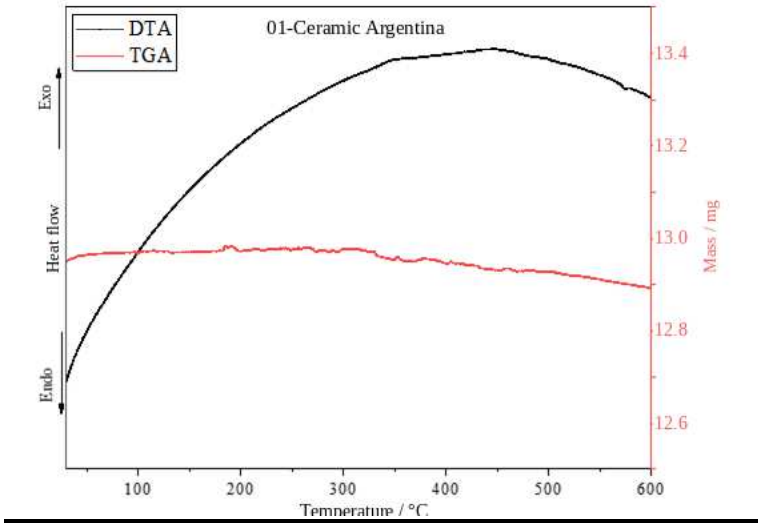

Source: Graph obtained from the test on the DTG-60 Simultaneous DTA-TG Apparatus at the Center for Spectroscopy and Molecular Structure (NEEM) of the UFJF Department of Chemistry (2026).

Overall, the Argentine ceramic block showed high thermal stability throughout the range, with very small mass loss and no significant decomposition events. This behavior indicates that the firing process was sufficient to chemically and mineralogically stabilize the minerals present in the clay, resulting in a thermally stable material, albeit without the full densification observed by SEM (item 5.1.2).

iii) BC BR vs. BC AR

Table 15 summarizes the correlation between the macroscopic properties and the thermogravimetric results of the ceramic blocks.

Table 15 – Summary of the analysis of macroscopic vs. thermogravimetric results for BC BR vs. BC AR.

	Properties	**THERMOGRAVIMETRY**

BC BR	ρ_{ap} = 2,072.94 kg/m³ AA = 22.67% f_{bk}= 1.44 MPa	Low mass loss throughout heating: confirms a mineralogical structure stabilized by firing; Absence of hydrated compounds: indicates that the high water absorption results from the open porosity of the material, not from reactions with moisture; High thermal stability: material little susceptible to transformations when subjected to heat.
BC AR	ρ_{ap} = 1,718 kg/m³ AA = 15% • f_{bk}= 1.2 MPa	Slight mass loss over the entire 25–600 °C range; Removal of surface moisture at the initial temperatures; Absence of significant thermal decomposition events; High thermal stability resulting from industrial firing.

Source: Prepared by the author (2026).

The thermogravimetric analysis revealed very similar thermal behavior for BC BR and BC AR, both characterized by slight mass loss over the entire heating range analyzed (25 °C to 600 °C) and by the absence of significant thermal decomposition events. In both materials, the only relevant mass loss occurred in the initial low-temperature range (up to 100 °C–150 °C), associated with the removal of free surface and interstitial water (Santos, 1989; Földvári, 2011), while the subsequent temperature ranges showed no significant events in the TGA/DTA curves. This pattern indicates that, from a thermal point of view, the main mineralogical transformation processes of the source clays had already been completed during the industrial firing of both blocks, leaving no unstable, hydrated or secondary thermal decomposition-prone phases in the final material.

The low magnitude of mass loss observed in both samples, together with the absence of abrupt thermal events in the DTA curves, is consistent with a firing process sufficient for the thermal stabilization of the clay minerals. This convergence between different characterization techniques (Raman and TGA) strengthens the interpretation that both BC BR and BC AR underwent firing processes sufficient for the chemical and mineralogical stabilization of the raw material, even though, as discussed in the SEM analysis, the physical consolidation between particles remained incomplete in both cases (Cultrone et al., 2004).

The similarity of the thermogravimetric results for the two ceramic blocks reinforces the central conclusion of the multi-technique characterization of this study: the differences observed in the macroscopic properties of BC BR and BC AR, especially water absorption (22.67% and 15%, respectively) and compressive strength

(1.44 MPa and 1.2 MPa), do not appear to result from differences in the efficiency of the thermal stabilization achieved by firing, since both materials proved to be thermally stable and to have similar mineral phases.

Thus, the thermogravimetric analysis indicates that firing was sufficient for the chemical and mineralogical stabilization of both materials, minimizing the effect of clay composition, although it did not achieve their full densification, and reinforces that the different behavior of the two ceramic blocks manifests mainly at the microstructural scale, associated with the morphology, distribution and connectivity of the pore network, as evidenced by the Scanning Electron Microscopy analyses (Cultrone *et al.*, 2004; Coletti *et al.*, 2016).

5.1.5 **Thermal conductivity**

Complementing the macroscopic (item 5.1.1), microscopic (item 5.1.2), mineralogical (item 5.1.3) and thermogravimetric (item 5.1.4) characterization of the ceramic blocks, thermal conductivity (λ) and thermal resistance (R) tests were carried out by the heat flow meter method, using a Netzsch HFM 446 Lambda Medium instrument, according to IRAM 1860 (IRAM, 2002). The tests were performed under steady-state conditions at the CECOVI Conductivity Laboratory of the Universidad Tecnológica Nacional, Facultad Regional Santa Fe (UTN-FRSF), Argentina, within the international scientific cooperation project between UFJF and UTN of which this dissertation is part (Barrientos Santini; Carrara, 2026).

i) BC BR

The Brazilian ceramic block samples (BC BR) could not be subjected to the thermal conductivity and thermal resistance test by the heat flow meter method, as they broke during transport to the CECOVI laboratory in Argentina. Therefore, λ and R values for the Brazilian ceramic material were not obtained experimentally by this method, which constitutes a logistical limitation of this comparative study, addressed in the analysis presented in item iii.

ii) BC AR

The Argentine ceramic blocks (BC AR) were tested under steady-state conditions at a mean test temperature of about 20 °C, the reference condition of IRAM

11601 (IRAM, 2004). The mean result is presented in Table 16, together with the value tabulated by that standard for a hollow ceramic block of similar dimensions and mass per unit area (IRAM 11601 indicates a mass per unit area of 69 kg/m² for this block). It should be noted that the ρap value presented in Table 16 (686.7 kg/m³) corresponds to the apparent density of the hollow block, obtained as the ratio between the dry mass and the gross volume of the half-section tested, including the holes; it therefore differs from the apparent density of 1,718 kg/m³ presented in Table 8, determined in the macroscopic test (item 5.1.1).

Table 16 – Mean thermal resistance result of BC AR (heat flow meter method).

SAMPLE	ρ_{ap} hollow block (kg/m³)	R (m²·K/W)	T (°C)
BC AR	686.7 (CV = 1.0%)	0.348 (CV = 3.9%)	≈ 20
IRAM 11601	–	0.350	20

Source: Adapted from Barrientos Santini and Carrara (2026).

The mean thermal resistance obtained for BC AR was 0.348 m²·K/W (CV ≈ 4%), practically coinciding (difference of less than 1%) with the value tabulated by IRAM 11601 for a ceramic block of similar dimensions and mass per unit area (0.350 m²·K/W). This result indicates good representativeness of the material tested relative to the reference standard values of its country of origin. It is important to note that, as reported in the test, the specimens had visible defects on both faces, including cracks and flatness irregularities, which may induce additional contact resistances or partially deflect the perpendicular linear heat flow, introducing some uncertainty into the individual results.

iii) BC BR vs. BC AR

A direct comparison between BC BR and BC AR in terms of thermal conductivity and thermal resistance could not be made, since the Brazilian specimens broke during transport, making testing by the heat flow meter method impossible (item i). This limitation prevents direct experimental validation of which material has the better insulating performance among the ceramic blocks of the two countries, as summarized in Table 17.

Table 17 – Summary of the analysis of macroscopic vs. thermal conductivity results for BC BR vs. BC AR.

	Properties	**Thermal conductivity (HFM)**
BC BR	ρ_{ap} = 2,072.94 kg/m³ AA = 22.67% f_{bk}= 1.44 MPa	Test not performed: specimens broke during transport to the CECOVI laboratory (Argentina)
BC AR	ρ_{ap} = 1,718 kg/m³ AA = 15% f_{bk}= 1.2 MPa	Mean thermal resistance R = 0.348 m²·K/W Agreement within < 1% of the value tabulated by IRAM 11601 (0.350 m²·K/W) Result consistent with the lower apparent density (item 5.1.1) and with the higher porosity identified by SEM

Source: Prepared by the author (2026), with data from Barrientos Santini and Carrara (2026).

Although a direct experimental comparison is not possible, the result obtained for BC AR can be interpreted in light of the macroscopic and microstructural analyses presented in items 5.1.1 and 5.1.2. BC AR has a lower apparent density (1,718 kg/m³) and a higher relative volume of irregular voids, identified by SEM, than BC BR (2,072.94 kg/m³). A lower apparent density generally tends to favor higher thermal resistance, as it reduces the number of continuous solid bridges available for heat conduction through the ceramic matrix, increasing the relative share of air trapped in the pores, a phase with much lower thermal conductivity than the solid ceramic matrix. In this sense, the value of R = 0.348 m²·K/W obtained for BC AR is compatible with its more porous microstructure, bearing in mind that, in hollow blocks, thermal resistance also depends to a large extent on the geometry and arrangement of the holes (air cells).

On the other hand, without the experimental data for BC BR, it is not possible to confirm whether its higher apparent density would in fact translate into lower thermal resistance when tested by the same method, nor to quantify the magnitude of such a difference. For future work, it is recommended that the Brazilian specimens broken in transport be replaced, so as to enable the direct comparison and complete, for this technique, the methodological triangulation initiated in this study.

5.1.6 **Summary of Results**

A summary of the main analyses of the data obtained in the macroscopic, microscopic and thermal studies carried out on the ceramic blocks (BC) is presented below:

a) Apparent density: ρ_{ap} BC BR > ρ_{ap} BC AR (2,072.94 kg/m³ > 1,718 kg/m³);

b) Water absorption: AA BC BR > AA BC AR (22.67% > 15%);

c) Compressive strength: fbk BC BR > fbk BC AR (1.44 MPa > 1.2 MPa);

d) The SEM tests indicate, for BC BR, a more uniform pore distribution, however with higher open porosity, possibly associated with the constituent minerals of the clay, which causes flaws in particle bonding. As these pores are open and interconnected, they favor capillary percolation and explain the higher water absorption of BC BR;

e) The SEM tests indicate, for BC AR, a less uniform pore distribution, with a high void content; however, these voids appear to be less interconnected, which tends to result in lower open porosity and, consequently, lower water absorption;

f) In the Raman and TGA tests, both samples showed mineralogical stabilization and thermal stability resulting from the firing of the material during the manufacturing process;

g) BC AR showed a mean thermal resistance of 0.348 m²·K/W, practically coinciding with the value tabulated by IRAM 11601 (0.350 m²·K/W), a result consistent with its lower apparent density and with the voids identified by SEM. For BC BR, thermal conductivity could not be determined, as the specimens broke during transport, which prevents a direct thermal comparison between the two ceramic blocks;

h) The type of clay and the mix composition used to produce the BC may affect porosity, but this effect tends to be minimized by firing during the manufacturing process, which may result in macroscopic properties that meet current standards, provided that firing is properly controlled.

5.2 CONCRETE BLOCKS (BCC)

5.2.1 **Macroscopic tests**

i) BCC BR

The Brazilian concrete blocks showed a mean apparent density of 2,191.04 kg/m³ (CV = 4.78%), a water absorption of 5.12% (CV = 21.80%), within the maximum

limit of 10% established by NBR 6136 (ABNT, 2016), and a mean compressive strength of 2.33 MPa (CV = 23.88%), which meets the minimum of 2.0 MPa required by the same standard for non-load-bearing blocks.

ii) BCC AR

The Argentine concrete blocks showed a mean apparent density of 1,980 kg/m³ (CV = 1.84%), lower than that observed for the Brazilian material. The mean water absorption was 8% (CV = 37.8%), higher than that of the Brazilian material, albeit with high scatter among the specimens tested. The mean compressive strength was 6.9 MPa (CV = 0.84%), markedly higher than that obtained for the Brazilian blocks and with a very low coefficient of variation. This value meets the minimum compressive strength requirement established by IRAM 11561-2 (IRAM, 2018) for non-load-bearing concrete blocks.

iii) BCC BR vs. BCC AR

Table 18 presents the mean results of the macroscopic tests performed on the Brazilian and Argentine concrete blocks.

Table 18 – Data from the tests performed on BCC BR vs. BCC AR.

SAMPLE	**DIMENSIONS** (cm)	ρ_{ap} (kg/m³)	**AA** (%)	f_{bk} (MPa)
BCC BR	8.94×18.75×39.01 (CV = 0.32%)	2,191.04 (CV = 4.78%)	5.12 (CV = 21.80%)	2.33 (CV = 23.88%)
BCC AR	8.95×18.78×38.68 (CV = 0.75%)	1,980 (CV = 1.84%)	8 (CV = 37.8%)	6.9 (CV = 0.84%)

Source: Prepared by the author (2026).

Comparing the two materials, it can be observed that the Brazilian concrete blocks had a higher apparent density than the Argentine ones, indicating a more compact cementitious matrix. This result is consistent with the lower water absorption observed in the Brazilian blocks (5.12%) compared with the Argentine ones (8%), reflecting the inverse relationship between density and porosity typical of cementitious materials.

The most marked difference between the two materials, however, was observed in compressive strength: the Argentine blocks reached a mean value almost three

times higher than the Brazilian ones (6.9 MPa vs. 2.33 MPa), in addition to a considerably lower coefficient of variation, which suggests greater uniformity and reliability of the Argentine production process. While the Brazilian block met the standard requirement by a narrow margin, the performance of the Argentine material suggests greater technological control in manufacturing and possibly a concrete mix with higher characteristic strength.

5.2.2 **Scanning Electron Microscopy (SEM)**

i) BCC BR

As shown in Figure 14, at 50x magnification the concrete block reveals distinct regions: the hardened cement matrix, the sand particles and the voids formed during manufacturing. Microcracks and small discontinuities are visible, common characteristics of this type of material.

At 250x magnification, a more continuous structure is observed, with sand particles dispersed within it. The pores are discontinuously distributed and vary in size and shape.

At 500x magnification, the separation between the hardened cementitious matrix and the aggregate particles can be seen more clearly. The matrix has a fine texture and the pores have irregular geometry and non-uniform distribution, which suggests air entrapment during molding, while the aggregates show angular morphology and well-defined interfaces.

Figure 14 – Magnifications of 50x, 250x, 500x, 1,000x and 2,000x of BCC BR.

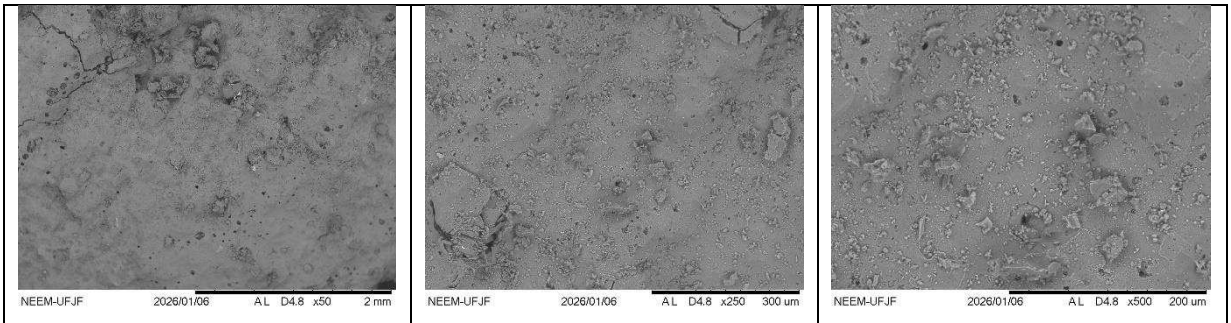

a) **50x**	b) **250x**	c) **500x**

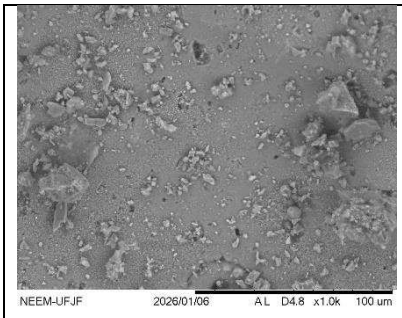

d) 1,000x

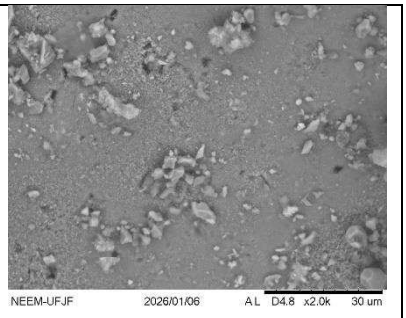

e) 2,000x

Source: Images obtained with the Hitachi TM3000 Tabletop Microscope at the Center for Spectroscopy and Molecular Structure (NEEM) of the UFJF Department of Chemistry (2026).

At 1,000x magnification, the angular grains appear embedded in a fine, compact matrix. The voids remain non-uniformly distributed.

At 2,000x magnification, details of the hardened cement matrix and small voids distributed over the surface are observed. The absence of extensive cracks at this scale is also noted, which points to initial structural integrity.

The correlation between the macroscopic tests and the SEM images of the two types of Brazilian blocks shows that the results of the two characterization scales are consistent with each other. BC BR has a porous microstructure with poorly bonded particles, which explains its higher water absorption capacity (22.67%) and its lower compressive strength (1.44 MPa). BCC BR, on the other hand, has a denser and more compact matrix, in which voids are partially filled during cement hardening, resulting in lower absorption (5.12%) and higher mechanical strength (2.33 MPa).

ii) BCC AR

Figure 15 presents the micrographs of BCC AR at magnifications from 50x to 2,000x.

Figure 15 – Magnifications of 50x, 250x, 500x, 1,000x and 2,000x of BCC AR.

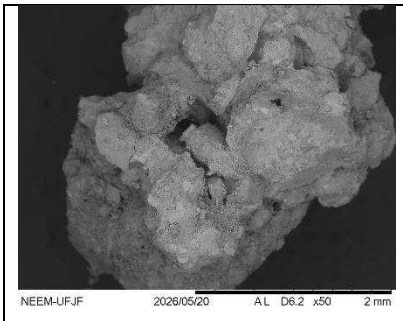

a) 50x

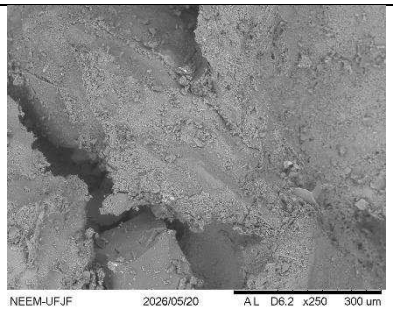

b) 250x

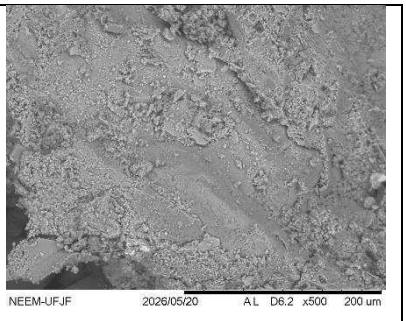

c) 500x

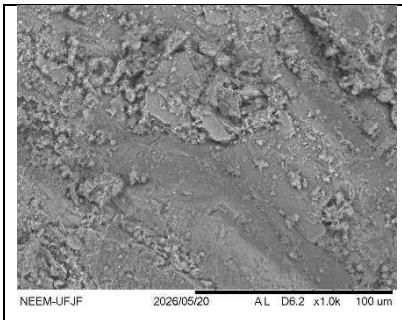

d) 1,000x

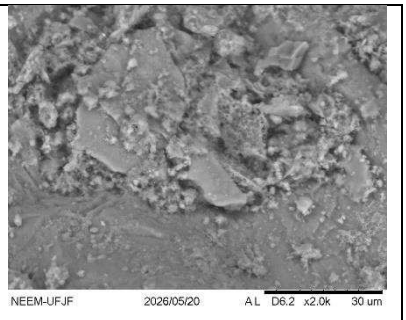

e) 2,000x

Source: Images obtained with the Hitachi TM3000 Tabletop Microscope at the Center for Spectroscopy and Molecular Structure (NEEM) of the UFJF Department of Chemistry (2026).

At 50x magnification, the concrete block shows large agglomerates separated by voids and discontinuities. This characteristic is understood to be related to the composition of the material.

At 250x magnification, the cement matrix is seen to surround the larger particles, with irregularly distributed pores. This variation may be related to the amount of water used in the mix, the degree of compaction and the conditions under which the block was cured.

At 500x magnification, the separation between the hardened cementitious matrix and the aggregates is observed more clearly. The matrix has a fine and heterogeneous texture, while the aggregates show rougher surfaces and well-defined edges. The pores have irregular shapes and a discontinuous distribution.

At 1,000x magnification, the structure shows a cementitious matrix composed of fine particles and irregular agglomerates distributed over the surface analyzed. Dense and porous regions alternate.

At 2,000x magnification, the details become evident, with agglomerates of cement matrix and small voids distributed over the surface. The rough texture observed can be considered the result of cement hydration. In addition, the distribution and connectivity of these small pores directly influence properties such as the permeability and durability of the block.

iii) BCC BR vs. BCC AR

Table 19 summarizes the comparison between the macroscopic properties and the SEM observations of BCC BR and BCC AR.

Table 19 – Summary of the analysis of macroscopic vs. SEM results for BCC BR vs. BCC AR.

	Properties	SEM
BCC BR	ρ_{ap} = 2,191.04 kg/m³ AA = 5.12% f_{bk} = 2.33 MPa	Dense and compact matrix; Small and discontinuous pores; Voids partially filled by hardened cement; Structural integrity preserved, with isolated microcracks and discontinuities.
BCC AR	ρ_{ap} = 1,980 kg/m³ AA = 8% f_{bk} = 6.9 MPa	Continuous cement matrix surrounding sand particles; Irregular and discontinuous pores; Well-distributed densified regions.

Source: Prepared by the author (2026).

The comparison between the concrete blocks reveals behavior opposite to that expected from the classical density–performance relationship: BCC BR showed a higher apparent density (2,191.04 kg/m³) and lower water absorption (5.12%) than BCC AR (1,980 kg/m³ and 8%, respectively), but a significantly lower compressive strength (2.33 MPa vs. 6.9 MPa for BCC AR). This result indicates that, for the concrete blocks evaluated, apparent density and water absorption are not direct predictors of mechanical performance, the latter possibly being more influenced by the quality of the interfacial transition zone between the hydrated cement paste and the aggregate, as well as by the degree of continuity and integrity of the cementitious matrix, aspects that can only be investigated by microstructural analysis such as SEM.

The SEM images indicate that BCC AR has a continuous cement matrix surrounding the aggregate particles, with densified regions well distributed over the surface analyzed, which suggests a more effective hydration process and better paste–aggregate bond, even in the presence of irregular and discontinuous pores.

BCC BR, on the other hand, despite having an apparently denser and more compact matrix at the microscopic scale, with small pores mostly filled by hardened cement, also revealed the presence of microcracks and isolated discontinuities in the matrix, factors that can act as stress concentration points. This observation is corroborated by the high coefficient of variation of the compressive strength of BCC BR (23.88%) compared with the very low CV of BCC AR (0.84%), which suggests that the homogeneity of the microstructure is decisive for the predictability and reliability of the mechanical performance of the material.

The results show that, in cementitious materials, mechanical strength is associated not only with the volume of voids in the matrix but mainly with their distribution and connectivity and with the quality of the paste–aggregate interface. BCC AR, despite its higher water absorption, indicative of higher accessible porosity, showed superior mechanical performance, which reinforces the hypothesis that cement hydration resulted in a more cohesive and uniform structural matrix, with more efficient bonding points between paste and aggregate.

In contrast, BCC BR, although macroscopically denser, showed greater internal heterogeneity and lower mechanical predictability, suggesting possible localized compaction flaws or irregular curing during the manufacturing process. This body of evidence reinforces the importance of microstructural characterization as an indispensable complementary tool for interpreting macroscopic tests, since isolated parameters such as apparent density may not directly reflect the actual mechanical performance of the material.

5.2.3 **Raman Spectroscopy**

The Raman spectra obtained for the concrete blocks are presented below, first for each block and then comparatively.

i) BCC BR

The Raman spectra of the concrete blocks reveal a different scenario. Taking as reference the peak at 1086 cm^{-1}, associated with the carbonate ion (CO_3^{2-}), the three samples show very different profiles (see Figure 16).

Figure 16 – Raman spectra of the BCC BR samples normalized to the 1086 cm^{-1} band.

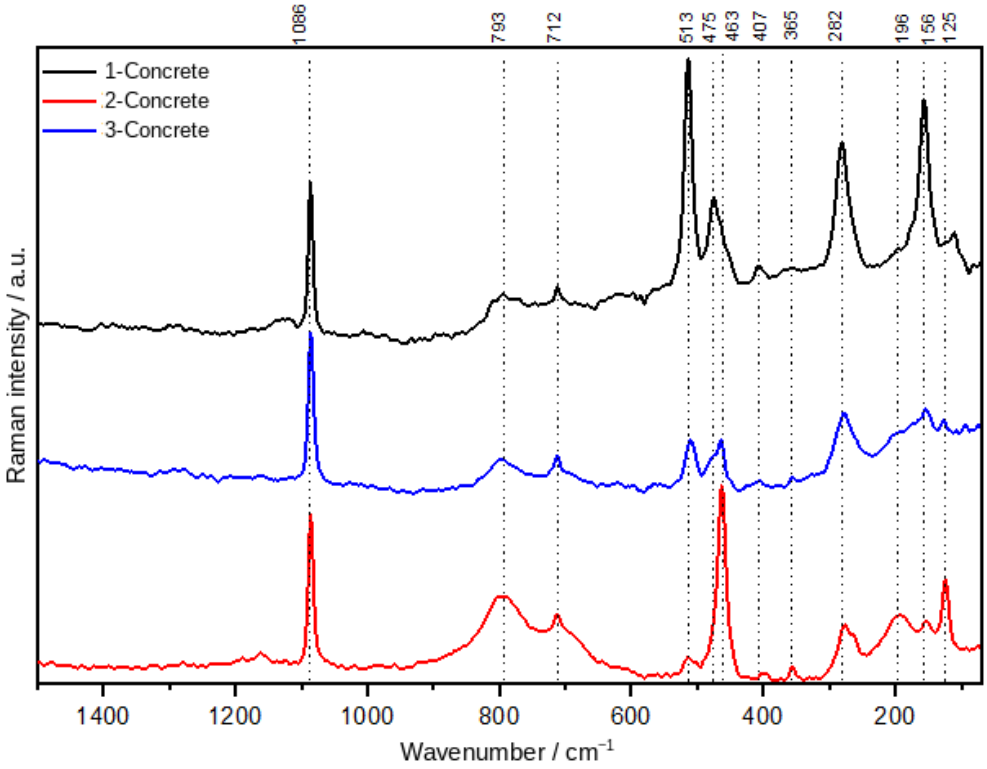

Source: Spectra obtained with the Bruker Multiram spectrometer at the Center for Spectroscopy and Molecular Structure (NEEM) of the UFJF Department of Chemistry, operating with an Nd:YAG laser (1064 nm) (2026).

The band assignments for the three BCC BR samples are detailed in Table 20.

Table 20 – Assignment of the Raman bands observed in the spectra of the BCC BR samples investigated.

v / cm^{-1}	Assignment
127	E mode: Quartz
156	L band: Carbonate
196	A_1 mode: Quartz
282	T band: Carbonate
365	Ca–O: Portlandite
407	δ(Si-O-Si): Tridymite
463	v_s(Si-O-Si): Quartz
475	v(T-O-T): Feldspar
513	v(T-O-T): Feldspar
712	δ(CO_3^{2-})
793	v(Si-O-Si): Quartz
1086	v(CO_3^{2-})

Where: T = Si or Al.

Source: Assignments made by the Center for Spectroscopy and Molecular Structure (NEEM) of the UFJF Department of Chemistry (2026).

Sample 1-Concrete stands out for its higher relative carbonate content, evidenced by the intense bands at 156 and 282 cm^{-1}, as well as the presence of bands at 475 and 513 cm^{-1}, assigned to the feldspar structure, suggesting a greater contribution of aluminosilicates to this composition than to the others.

Sample 3-Concrete shows higher intensity in the peaks associated with quartz and tridymite, identified at 127, 196, 463 and 793 cm^{-1}, indicating a greater share of sand in the composition. Sample 2-Concrete shows intermediate behavior, with balanced signals between carbonates and silicates. The differences in carbonate content, however, could not be compared with thermogravimetry, since the decomposition of these phases occurs above 600 °C, the upper limit of the range tested.

In the 355–365 cm^{-1} region, the presence of portlandite ($Ca(OH)_2$), a product of the reaction of cement with water, is observed. The bands near 460–465 cm^{-1} are assigned to quartz, indicating the contribution of mineral aggregates to the composition of the block.

At higher wavenumbers, at 712 and 1086 cm^{-1}, bands associated with calcite stand out, showing that part of the cement compounds reacted with atmospheric carbon dioxide over time, a process known as carbonation (see Table 21).

Table 21 – Interpretation of the BCC BR band assignments.

Range (cm^{-1})	**Associated phase**	**Interpretation**
150–300	Carbonates	Carbonate compounds present in the cementitious matrix, with a poorly ordered structure
355–365	Portlandite	Product of the reaction of cement with water; confirms hardening of the material by chemical reaction
460–465	Quartz (Si – O)	Fine aggregate (sand) present in the composition of the block
710–715	Calcite	Product of carbonation (reaction of cement compounds with atmospheric CO_2)
793	Quartz	Fine aggregate (sand) present in the composition of the block

Source: Prepared by the author (2026).

ii) BCC AR

The Raman spectra of BCC AR, normalized to the band at 1086 cm^{-1}, associated with the carbonate ion (CO_3^{2-}), reveal a more varied and complex mineralogical composition than that of BC AR (Figure 17).

Figure 17 – Raman spectra of BCC AR normalized to the 1086 cm^{-1} band.

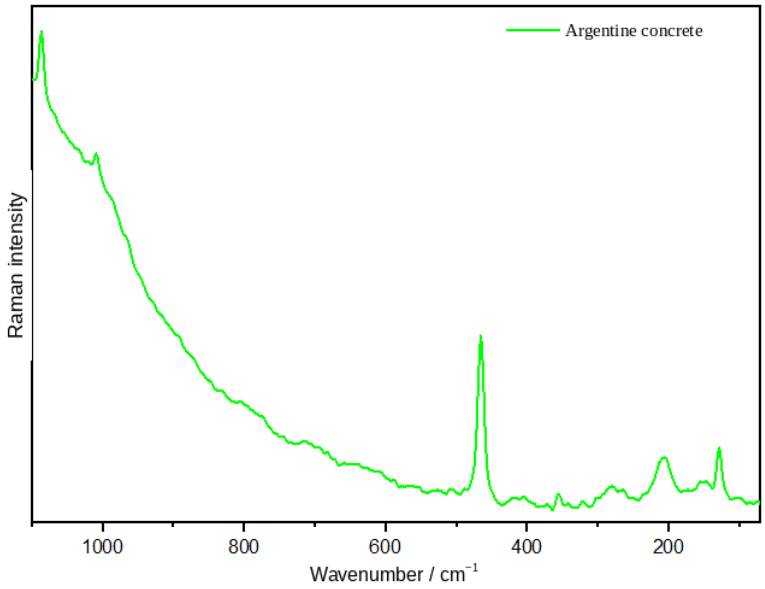

Source: Spectra obtained with the Bruker Multiram spectrometer at the Center for Spectroscopy and Molecular Structure (NEEM) of the UFJF Department of Chemistry, operating with an Nd:YAG laser (1064 nm) (2026).

The assignments of the vibrational bands observed in the concrete block are presented in Table 22.

Table 22 – Assignment of the Raman bands observed in the spectra of BCC AR.

v / cm^{-1}	Assignment
125	E mode: Quartz
157	A_g mode: Feldspar
206	A_1 mode: Quartz
263	E mode: Quartz
282	L band: Carbonate
358	δ(Si-O-Si): Quartz
407	v_s(Fe-O): Hematite
463	v_s(Si-O-Si): Quartz
475	v(T-O-T): Feldspar
513	v_s(Al-O-Al): Feldspar
712	δ(O-C-O)
793	v_s(Si-O): Quartz
1010	$v_s(SO_4^{2-})$: Gypsum
1086	$v_s(CO_3^{2-})$: Carbonate

Where: T = Si or Al.

Source: Assignments made by the Center for Spectroscopy and Molecular Structure (NEEM) of the UFJF Department of Chemistry (2026).

The bands at 125, 206, 263, 358, 463 and 793 cm^{-1} identified in the BCC AR sample are associated with quartz, indicating a significant contribution of sand as a constituent aggregate of the block.

The bands identified at approximately 475 and 513 cm^{-1} indicate the presence of feldspars, minerals of the aluminosilicate group, also derived from the aggregates used in manufacturing.

The peak at 282 cm^{-1} and the band at 712 cm^{-1} reinforce the presence of carbonate compounds distributed throughout the matrix.

The band at approximately 1010 cm^{-1}, assigned to gypsum, suggests the incorporation of sulfate compounds into the composition of the cementitious system analyzed.

The bands observed have a relatively broader and less defined profile than those of the ceramic materials, a behavior consistent with the partially amorphous and heterogeneous nature typical of the hydrated cementitious matrix (see Table 23).

Table 23 – Interpretation of the BCC AR band assignments.

Range (cm^{-1})	Associated phase	Interpretation
125–263	Quartz and Feldspar	Minerals derived from the aggregates used to manufacture the block, mainly sand.
282	Carbonate	Carbonate compounds present in the cementitious matrix.
358–513	Quartz, Feldspar and Hematite	Aluminosilicates and silicate minerals from the aggregates; Indicate mineralogical diversity in the composition.
712–793	Carbonate and Quartz	Carbonate and silicate compounds; The presence of carbonate in this range shows carbonation of the matrix.
1010	Gypsum	Presence of sulfate compounds, possibly related to the cement manufacturing process.
1086	Carbonate	Predominant carbonate phase in the material; most intense peak in the spectrum.

Source: Prepared by the author (2026).

The detailed analysis of the Raman bands shows the presence of different mineral phases associated with both the cementitious matrix and the aggregates in the concrete. The bands between approximately 100 and 300 cm^{-1} are mainly related to vibrations associated with quartz and carbonates, reflecting the mineralogical contribution of the aggregates and of the carbonate phases present in the system.

In the region between approximately 350 and 550 cm^{-1}, contributions associated with quartz and feldspars are observed, indicating the presence of aluminosilicates distributed in the composition of the material. The bands at around 475 and 513 cm^{-1} reinforce the participation of these mineral phases in the concrete structure.

At higher wavenumbers, the bands associated with carbonates and gypsum stand out. The band at approximately 1010 cm^{-1} indicates sulfate compounds in the composition of the material, while the band at 1086 cm^{-1} confirms the significant contribution of carbonate phases.

The body of spectral evidence is consistent with a multiphase, partially amorphous and mineralogically heterogeneous cementitious system, typical of hydrated cementitious materials.

iii) BCC BR vs. BCC AR

Table 24 summarizes the comparison between the macroscopic properties and the main Raman spectroscopy results of BCC BR and BCC AR.

Table 24 – Summary of the analysis of macroscopic vs. Raman results for BCC BR vs. BCC AR.

	Properties	**RAMAN**
BCC BR	ρ_{ap} = 2,191.04 kg/m³ AA = 5.12% f_{bk} = 2.33 MPa	Presence of portlandite and carbonates; Less ordered structure; Variable composition among samples; Signs of carbonation.
BCC AR	ρ_{ap} = 1,980 kg/m³ AA = 8% f_{bk} = 6.9 MPa	Presence of quartz, feldspars, carbonates and gypsum; Hydrated multiphase cementitious system; Evidence of matrix carbonation; Mineralogically heterogeneous and partially amorphous structure.

Source: Prepared by the author (2026).

The Raman spectra of BCC BR show the presence of phases characteristic of cement hydration and carbonation, notably bands assigned to portlandite (355–365 cm^{-1}) and to carbonate compounds such as calcite, at 156, 282, 712 and 1086 cm^{-1}. A particularly relevant aspect is the marked compositional heterogeneity observed among the three BCC BR samples themselves, which showed different proportions of carbonates, silicates and aluminosilicates, unlike the homogeneous behavior found in the ceramic blocks. This variability among samples is consistent with the high coefficient of variation obtained for the compressive strength of BCC BR (23.88%), suggesting that carbonation did not occur uniformly across the specimens evaluated.

BCC AR, in turn, showed Raman spectra with greater mineralogical diversity, revealing not only carbonate phases but also quartz, feldspars and gypsum, the latter associated with the presence of sulfate compounds in the composition of the cementitious system. The bands obtained were relatively broader and less defined than those observed in the ceramic blocks, a behavior consistent with the partially amorphous nature of the hydrated cementitious matrix and with the coexistence of multiple mineral phases derived from both the cement and the incorporated aggregates. Notably, despite this mineralogical heterogeneity intrinsic to the system, BCC AR showed the lowest coefficient of variation in compressive strength of all the materials analyzed (0.84%), which suggests that the diversity of phases identified reflects the natural and expected composition of a multiphase concrete rather than an inconsistency or flaw in the manufacturing process.

The comparison between the Raman profiles of the two concrete blocks makes it possible to associate, albeit indirectly, the compositional differences identified with the mechanical performance observed macroscopically. BCC BR, despite showing signs of cement hydration (portlandite) and a higher apparent density, also showed signs of carbonation and marked compositional variability among samples, factors that may compromise the homogeneity of the cementitious matrix and, consequently, its mechanical strength (2.33 MPa).

BCC AR, on the other hand, despite its higher water absorption and more complex mineralogical system, showed considerably higher compressive strength (6.9 MPa) and greater statistical uniformity in the mechanical results, suggesting a more uniform cementitious matrix with a more regular distribution of the phases formed. These findings reinforce that, for cementitious materials, mechanical strength is not associated solely with apparent density or with the number of phases present but

possibly with the quality and uniformity of the cementitious matrix and with the degree of microstructural development of the matrix, aspects shown in a complementary manner by the SEM and Raman techniques.

5.2.4 **Thermogravimetry**

The thermogravimetric curves obtained for the concrete blocks are presented below, first for each block and then comparatively.

i) BCC BR

BCC BR showed thermal behavior different from that observed for BC BR, as shown in Figure 18.

From Figure 18, it can be observed that:

i) 25 °C to 120 °C: A mass reduction is observed, attributed to the evaporation of free water and moisture retained in the pores of the material. The low intensity of this event suggests that the block has a relatively stable structure, with a moderate amount of water retained in its internal voids.
ii) 120 °C to 300 °C: A gradual mass loss is observed, associated with the decomposition of the compounds formed during the reaction of cement with water. This stage is consistent with the presence of the main products responsible for the cohesion of the cementitious matrix.
iii) 300 °C to 450 °C: The mass loss remains continuous, still associated with the progressive decomposition of the remaining hydrated compounds. The absence of sharp peaks in this region suggests gradual decomposition, consistent with a relatively homogeneous cementitious matrix in this temperature range.
iv) 450 °C to 600 °C: From approximately 450 °C onwards, an increase in the rate of mass loss is observed, related to the decomposition of portlandite ($Ca(OH)_2$), a product of the reaction of cement with water, which releases water when heated. The continued mass loss up to 600 °C suggests that the decomposition of this phase was not yet complete within the temperature range analyzed.

Figure 18 – TGA and DTA curves of BCC BR.

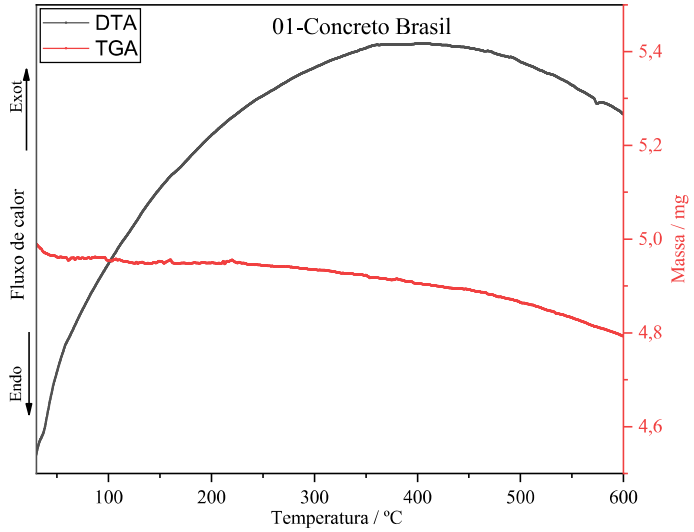

Source: Graph obtained from the test on the DTG-60 Simultaneous DTA-TG Apparatus at the Center for Spectroscopy and Molecular Structure (NEEM) of the UFJF Department of Chemistry (2026).

Thus, the Brazilian concrete block showed a gradual mass loss distributed throughout heating, with no abrupt events, indicating that the compounds present in the material decompose progressively as the temperature increases. This behavior is typical of cementitious materials and is directly related to the presence of compounds formed by the reaction of cement with water.

ii) BCC AR

Figure 19 presents the thermogravimetric analysis (TGA) and differential thermal analysis (DTA) curves of the Argentine concrete block.

Figure 19 – TGA and DTA curves of BCC AR.

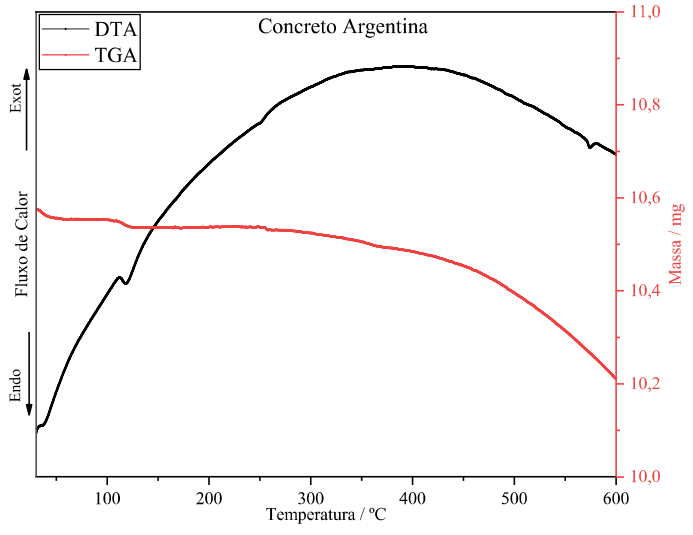

Source: Graph obtained from the test on the DTG-60 Simultaneous DTA-TG Apparatus at the Center for Spectroscopy and Molecular Structure (NEEM) of the UFJF Department of Chemistry (2026).

From Figure 19, it can be observed that:

i) 25 °C to 150 °C: A slight mass loss is observed, associated with the evaporation of free water and moisture retained in the pores of the material.
ii) 150 °C to 300 °C: The mass loss continues moderately, associated with the removal of water chemically bound to the products of cement hydration.
iii) 300 °C to 450 °C: The mass loss proceeds gradually, with no abrupt events. The DTA curve begins to show a tendency to level off near its maximum value, suggesting that the main dehydration events of the hydrated compounds are approaching completion in this region.
iv) 450 °C to 600 °C: The highest rate of mass loss recorded during the test is observed, showing the continued decomposition of the hydrated cement products. The TGA curve has a steeper slope in this region, while the DTA curve indicates the occurrence of important thermal transformations.

Overall, the Argentine concrete block showed thermogravimetric behavior typical of cementitious materials, with continuous and progressive mass loss throughout heating, associated with the removal of free water and the decomposition of the cement hydration products. Unlike BC AR, which proved to be thermally stable, the concrete block showed greater sensitivity to heating, reflecting the presence of hydrated compounds in its structure.

iii) BCC BR vs. BCC AR

Table 25 summarizes the comparison between the macroscopic properties and the thermogravimetric results of BCC BR and BCC AR.

Table 25 – Summary of the analysis of macroscopic vs. thermogravimetric results for BCC BR vs. BCC AR.

	Properties	**THERMOGRAVIMETRY**

BCC BR	ρ_{ap} = 2,191.04 kg/m³ AA = 5.12% f_{bk} = 2.33 MPa	Gradual and continuous mass loss: associated with the progressive decomposition of the compounds formed by cement hydration; Events consistent with C-S-H and portlandite (the latter identified by Raman): compounds associated with the lower water absorption of the material; Greater thermal sensitivity: consistent with the greater variability observed in the physical tests (high CV)
BCC AR	ρ_{ap} = 1,980 kg/m³ AA = 8% f_{bk} = 6.9 MPa	Continuous mass loss throughout heating, intensifying from 450 °C; Removal of free and adsorbed water at the initial temperatures; Progressive dehydration of the cement hydration products (C-S-H); Mass loss between 450 °C and 600 °C consistent with the dehydroxylation of portlandite (phase not identified by Raman in this material); Behavior typical of a hydrated cementitious matrix.

Source: Prepared by the author (2026).

The thermogravimetric analysis confirmed, for both concrete blocks, a thermal decomposition pattern characteristic of hydrated cementitious systems, with mass loss distributed over the entire heating range analyzed, in marked contrast with the high thermal stability observed in the ceramic blocks. In both cases, three consistent thermal events were identified: (i) evaporation of free and surface water up to approximately 120 °C–150 °C; (ii) gradual decomposition of the cement hydration products, including calcium silicate hydrate (C-S-H), between 150 °C and 450 °C; and (iii) intensification of mass loss between 450 °C and 600 °C, associated with the dehydroxylation of portlandite ($Ca(OH)_2$). In BCC BR, the assignment of event (iii) to portlandite is consistent with the identification of this phase by Raman spectroscopy; in BCC AR, however, portlandite was not identified by Raman, so this assignment should be understood as a hypothesis.

Despite the similar overall pattern, relevant differences were observed in the distribution of mass loss between the two materials. BCC BR showed a more pronounced mass loss in the intermediate range (120 °C to 450 °C), associated with the progressive decomposition of the hydration products, with no abrupt peaks, suggesting a relatively homogeneous matrix in this temperature range.

BCC AR, on the other hand, showed the highest rate of mass loss precisely in the final range (450 °C to 600 °C), with a steeper slope in the TGA curve and more evident thermal transformations in the DTA curve, a behavior consistent with the dehydroxylation of portlandite. However, this phase was not identified by Raman

spectroscopy in BCC AR, so the interpretation that this material contains more portlandite and, consequently, reached a more advanced degree of cement hydration than BCC BR should be considered a hypothesis, to be confirmed by complementary techniques such as X-ray diffraction.

The higher mass loss of BCC AR between 450 °C and 600 °C, together with the multiphase cementitious matrix identified by Raman and the structural continuity observed by SEM, is consistent with the superior mechanical performance of this material (6.9 MPa) compared with BCC BR (2.33 MPa). If the hypothesis of a higher degree of cement hydration is confirmed, this factor would contribute to a more cohesive matrix and a more efficient bond between paste and aggregate. It should be noted, however, that the higher water absorption of BCC AR (8% vs. 5.12% for BCC BR) cannot be attributed to a higher degree of hydration, since greater formation of hydration products tends to refine the pore structure of the paste and seal part of the pores, reducing capillary absorption. This difference may be related to other factors, such as the concrete mix proportions, the aggregate grading and the degree of compaction of the blocks, hypotheses that were not verified in this study. Thus, thermogravimetry completes the analytical triangulation with SEM and Raman by indicating that the characteristics of the cementitious matrix, and not only apparent density or apparent void volume, are associated with the difference in mechanical strength observed between the concrete blocks evaluated.

5.2.5 **Thermal conductivity**

To evaluate the thermal conductivity of the concrete matrix without the effect of the air cells of the hollow blocks, flat concrete slabs from both countries were tested by the same heat flow meter method described in item 5.1.5. In the Argentine case, the slabs were obtained from the same blocks characterized in items 5.2.1 to 5.2.4 by mechanically removing the internal webs; in addition, the Argentine hollow blocks were tested as half-sections, preserving the air cells, to determine the thermal resistance of the component.

i) BCC BR

The Brazilian flat concrete slabs showed a mean apparent density of 1,778.8 kg/m³ and a mean thermal conductivity of 0.939 W/m·K at a mean test temperature of approximately 21 °C (Table 26). This value is about 33% lower than that tabulated by

ABNT NBR 15220-2 for no-fines (cavernous) concrete in the 1,700 to 2,100 kg/m³ range (λ = 1.400 W/m·K), which indicates that the standard value is conservative for the material tested. No equivalent test was performed on the Brazilian hollow blocks.

ii) BCC AR

The Argentine flat concrete slabs showed a mean apparent density of 1,734.7 kg/m³ and a mean thermal conductivity of 0.979 W/m·K, practically coinciding with the value tabulated by IRAM 11601 for normal-weight concrete with stone aggregates at 1,800 kg/m³ (λ = 0.970 W/m·K), with a deviation of less than 1%. The hollow blocks, in turn, showed a mean thermal resistance of 0.178 m²·K/W (CV ≈ 5%), about 5% higher than the reference value of the same standard for a concrete block of similar dimensions (0.17 m²·K/W). The results are summarized in Table 26.

Table 26 – Mean thermal conductivity and thermal resistance results of the concrete blocks (heat flow meter method).

SAMPLE	TEST CONDITION	ρ_{ap} (kg/m³)	λ (W/m·K)	R (m²·K/W)
BCC BR	Flat slab (dense matrix)	1,778.8	0.939	–
BCC AR	Flat slab (dense matrix)	1,734.7	0.979	–
BCC AR	Hollow block (half-section)	1,317.3	–	0.178
ABNT NBR 15220-2	No-fines (cavernous) concrete	1,700 to 2,100	1.400	–
IRAM 11601	Normal-weight concrete with stone aggregates	1,800	0.970	–
IRAM 11601	Hollow concrete block	–	–	0.17

Source: Adapted from Barrientos Santini and Carrara (2026).

iii) BCC BR vs. BCC AR

In the thermal conductivity tests performed on the dense concrete matrix, without air cells, the mean thermal conductivity was 0.939 W/m·K for BCC BR and 0.979 W/m·K for BCC AR, a difference of only about 4%, which indicates that the cementitious matrices of the two countries have practically equivalent intrinsic thermal properties for similar densities, between 1,700 and 1,800 kg/m³.

This result is particularly relevant in light of the marked differences in mechanical and microstructural performance identified between BCC BR and BCC AR in items 5.2.1 to 5.2.4: although BCC AR has a compressive strength almost three times higher than BCC BR (6.9 MPa vs. 2.33 MPa) and a more continuous cementitious matrix, observed by SEM, in addition to the hypothesis of a higher degree of cement hydration

raised by thermogravimetry, its thermal conductivity in the dense matrix is not lower than that of the Brazilian material — it is, in fact, slightly higher. This finding reinforces the conclusion, discussed in item 5.3, that, for the concretes evaluated, the quality and uniformity of the cementitious matrix mainly govern mechanical performance, whereas the thermal performance of the solid matrix proved to be little sensitive to these microstructural differences.

Regarding standard compliance, a different behavior is observed between the two countries: the Argentine standard IRAM 11601 reproduced very faithfully the value measured for the dense Argentine concrete, with a deviation of less than 1%, whereas the Brazilian standard ABNT NBR 15220-2 adopts a markedly conservative value (1.400 W/m·K), about 43% to 49% higher than the experimentally measured means in this study. In practical terms, this means that Brazilian designs that use only the value tabulated in NBR 15220-2, without laboratory characterization, tend to overestimate heat transfer through dense concrete elements, which may result in envelope designs that are more conservative — and potentially less cost-efficient — than the physical reality of the materials would allow. Table 27 summarizes the comparison between the macroscopic properties and the thermal conductivity results of BCC BR and BCC AR.

Table 27 – Summary of the analysis of macroscopic vs. thermal conductivity results for BCC BR vs. BCC AR.

	Properties	**THERMAL CONDUCTIVITY (HFM)**
BCC BR	ρ_{ap} = 2,191.04 kg/m³ AA = 5.12% f_{bk} = 2.33 MPa	Mean λ of the flat slabs (without air cells): 0.939 W/m·K About 33% lower than the conservative value tabulated by ABNT NBR 15220-2 (1.400 W/m·K)
BCC AR	ρ_{ap} = 1,980 kg/m³ AA = 8% f_{bk} = 6.9 MPa	Mean λ of the slabs extracted from the hollow blocks: 0.979 W/m·K Deviation < 1% from the value tabulated by IRAM 11601 (0.970 W/m·K)

Source: Prepared by the author (2026), with data from Barrientos Santini and Carrara (2026).

Thus, the characterization of thermal conductivity by the heat flow meter method acts as a complementary element to the analytical triangulation (SEM, Raman and TGA) performed for the concrete blocks, showing that, although the quality of the cementitious matrix and the resulting microstructure appear decisive for mechanical

performance, the thermal conductivity of the dense concrete matrix remains relatively stable between the two countries, with no apparent relationship to the microstructural differences observed.

5.2.6 **Summary of results**

A summary of the main analyses of the data obtained in the macroscopic, microscopic and thermal studies carried out on the concrete blocks (BCC) is presented below:

a) Apparent density: ρap BCC BR > ρap BCC AR (2,191.04 kg/m³ > 1,980 kg/m³);
b) Water absorption: AA BCC BR < AA BCC AR (5.12% < 8%);
c) Compressive strength: fbk BCC BR < fbk BCC AR (2.33 MPa < 6.9 MPa);
d) For BCC BR, SEM shows a compact matrix, but with isolated microcracks and discontinuities; Raman indicates compositional heterogeneity among the samples and signs of carbonation, which is consistent with the high scatter in compressive strength (CV = 23.88%);
e) For BCC AR, SEM shows a continuous cementitious matrix surrounding the aggregates; Raman reveals a multiphase system (quartz, feldspars, carbonates and gypsum); and TGA indicates a higher mass loss between 450 °C and 600 °C, consistent with the dehydroxylation of portlandite, a phase not identified by Raman in this material, which only allows the hypothesis of a more advanced degree of cement hydration to be raised; these results are consistent with the higher strength and low scatter of the results (CV = 0.84%);
f) Both blocks showed continuous mass loss throughout heating, a behavior typical of hydrated cementitious matrices and different from the thermal stability observed in the ceramic blocks;
g) In the dense matrix (flat slabs), thermal conductivity was practically equivalent between the two countries (λ = 0.939 W/m·K for BCC BR and 0.979 W/m·K for BCC AR, a difference of about 4%). IRAM 11601 (0.970 W/m·K) reproduces the measured value with a deviation of less than 1%, while NBR 15220-2 (1.400 W/m·K) adopts a conservative value. The Argentine hollow concrete blocks showed a mean thermal resistance of 0.178 m²·K/W, about half of that obtained for BC AR (0.348 m²·K/W);
h) Thus, in the concrete blocks, the quality and uniformity of the cementitious matrix, possibly associated with the manufacturing and curing process, appear to govern mechanical performance, but have little effect on the thermal

conductivity of the matrix. Both blocks met the minimum compressive strength requirements of the respective standards for non-load-bearing blocks.

i)

5.3 ANALYSES

Table 28 presents the comparative synthesis of the four materials studied, bringing together the results of the macroscopic, microscopic and thermal tests.

Table 28 – Comparative synthesis: macroscopic, microscopic and thermal tests.

Property	BC BR	BCC BR	BC AR	BCC AR
ρ_{ap} (kg/m³)	2,072.94	2,191.04	1,718	1,980
AA (%)	22.67	5.12	15	8
f_{bk} (MPa)	1.44	2.33	1.2	6.9
SEM	Homogeneous mass; partially bonded particles; open and interconnected pores.	Compact matrix; small and discontinuous pores; localized microcracks.	Heterogeneous structure; large irregular voids; low degree of densification.	Continuous matrix surrounding the aggregate; well-distributed irregular pores.
Raman	Hematite, quartz and anatase; crystalline and stable material; absence of hydrated phases.	Portlandite, carbonates and quartz; compositional heterogeneity among samples.	Hematite, quartz and anatase; crystalline and stable material.	Quartz, feldspar, carbonates and gypsum; multiphase, partially amorphous system.
Thermogravimetry	Minimal mass loss; high thermal stability between 25 °C and 600 °C.	Gradual and continuous loss; intensification above 450 °C (decomposition of portlandite).	Slight mass loss; high thermal stability.	Continuous loss, more intense between 450 °C and 600 °C (consistent with dehydroxylation of portlandite, not identified by Raman; hypothesis of a higher degree of hydration).
Thermal conductivity (HFM)	Not tested (specimens broke during transport).	Flat slabs: λ = 0.939 W/m·K (NBR 15220-2: 1.400 W/m·K).	Hollow block: R = 0.348 m²·K/W (IRAM 11601: 0.350 m²·K/W).	Flat slabs: λ = 0.979 W/m·K; hollow block: R = 0.178 m²·K/W (IRAM 11601: 0.970 W/m·K and 0.17 m²·K/W).
Mechanistic synthesis	Incomplete consolidation due to insufficient sintering; high open porosity.	Good overall densification, but compositional heterogeneity (carbonates and silicates) among samples.	Incomplete consolidation due to insufficient sintering; marked structural heterogeneity.	More continuous matrix (hypothesis of more advanced hydration, to be confirmed); best mechanical performance of the set.

Source: Prepared by the author (2026).

Comparing the two ceramic blocks directly, BC BR is 20.7% denser than BC AR (2,072.94 kg/m³ vs. 1,718 kg/m³) and yet absorbs 51% more water (22.67% vs. 15%), a result that contradicts the expectation that higher density implies lower accessible porosity (Santos, 1989; Cultrone *et al.*, 2004). Compressive strength follows density, with BC BR being 20% stronger than BC AR (1.44 MPa vs. 1.2 MPa), a much smaller difference than that observed in absorption.

The SEM images help explain this apparent paradox: both materials show incomplete consolidation of the clay particles, angular grains and few contact points, evidencing insufficient sintering during firing in both countries, but the pore distribution pattern differs. BC AR shows larger and more irregular voids coexisting with more compact regions, while BC BR has more interconnected pores, which favors capillary percolation of water even in a matrix of higher density.

Raman spectroscopy showed qualitatively similar mineralogical compositions for the two materials (hematite, quartz and anatase), with no hydrated or carbonate phases and with differences in the relative proportions of the phases associated with the type of clay and the mix composition. Thermogravimetry reinforces this reading, with both blocks losing a very small fraction of mass up to 600 °C, showing equivalent thermal stability. It is concluded that the type of clay and the mix composition influence the porosity of the blocks, but this effect is minimized by firing, so that the difference in behavior between BC BR and BC AR is expressed mainly in the connectivity of the pore network.

Among the concrete blocks, the pattern is reversed: BCC BR is only 10.7% denser than BCC AR (2,191.04 kg/m³ vs. 1,980 kg/m³) and absorbs 36% less water (5.12% vs. 8%), a behavior consistent with the classical relationship between density and porosity. However, the compressive strength of BCC AR is almost three times that of BCC BR (6.9 MPa vs. 2.33 MPa), a discrepancy that density alone does not explain.

SEM helps explain this discrepancy: BCC AR has a continuous cementitious matrix, well distributed around the aggregate, with homogeneously densified regions, while BCC BR, despite being denser, shows isolated microcracks and discontinuities that can act as stress concentrators. Raman reveals greater compositional heterogeneity among the BCC BR samples themselves (variation in the proportions of carbonates, silicates and aluminosilicates), consistent with its high coefficient of variation in strength (23.88%), whereas BCC AR, despite being mineralogically more diverse (quartz, feldspar, carbonates and gypsum), had the lowest strength CV of all the materials studied (0.84%). Thermogravimetry completes the picture: BCC AR shows a higher mass loss between 450 °C and 600 °C, consistent with the dehydroxylation of portlandite; since this phase was not identified by Raman in this material, the hypothesis of a more advanced degree of cement hydration still requires confirmation. It should be noted that the higher water absorption of BCC AR does not result from greater hydration, which tends to refine the paste and reduce capillary

absorption, and may be associated with the mix proportions, the aggregate grading or the degree of compaction of the blocks, hypotheses not verified in this study. Thus, for the concretes evaluated, mechanical strength is associated not with apparent density but with the quality and uniformity of the cementitious matrix.

The BC BR vs. BC AR and BCC BR vs. BCC AR comparisons reveal that the microstructure formation mechanisms (sintering by firing in the ceramic blocks, Portland cement hydration in the concrete blocks) respond differently to the variation in density between the two countries. In the ceramic blocks, the higher density of BC BR did not translate into lower absorption or a large gain in strength, since the limiting factor appears to be the connectivity of the pore network rather than the total void volume. In the concretes, the higher density of BCC BR also did not translate into higher strength, because the determining factor appears to be the quality of the cementitious matrix and of the paste–aggregate transition zone, rather than the apparent density of the matrix. In both families of materials, therefore, apparent density proved to be a weak predictor of performance, reinforcing that microstructural characterization (SEM, Raman and TGA) is indispensable for correctly interpreting the macroscopic results.

It is also worth noting that the magnitude of the effect of replacing ceramic with concrete within each country is not the same: mechanical strength increases by 62% in Brazil and by 475% in Argentina when switching from ceramic to concrete blocks, while water absorption decreases by 77% in Brazil and by 47% in Argentina, showing that the regional production process, and not only the type of material, also shapes the intensity of these responses.

Regarding thermal performance, the heat flow meter tests made it possible to quantify what the previous analyses only suggested. In Argentina, where both types of block could be tested as hollow units, the ceramic block showed a thermal resistance (0.348 $m^2 \cdot K/W$) practically twice that of the concrete block (0.178 $m^2 \cdot K/W$), despite its smaller thickness, a result consistent with the lower density and higher porosity of the ceramic matrix, although the geometry of the cavities also contributes to the difference. In the dense concrete matrix, thermal conductivity was practically the same in the two countries (0.939 and 0.979 $W/m \cdot K$), despite the marked differences in mechanical strength, showing that the microstructural differences between the concretes had little effect on the thermal performance of the cementitious matrix.

As for the standards, the values tabulated by IRAM 11601 proved very close to those measured (deviations of less than 1% for BC AR and for the Argentine concrete slabs, and of about 5% for the hollow concrete blocks), while ABNT NBR 15220-2 adopts for concrete a conductivity (1.400 W/m·K) between 43% and 49% higher than the measured means. The absence of results for BC BR, whose specimens broke during transport, makes it impossible to confirm whether the same behavior occurs among the Brazilian blocks.

6 CONCLUSIONS

This research comparatively investigated the properties of ceramic blocks (BC) and concrete blocks (BCC) used in non-load-bearing masonry in Juiz de Fora (Brazil) and Santa Fe (Argentina), integrating macroscopic tests (apparent density, water absorption and compressive strength), microstructural and mineralogical characterization techniques (SEM, Raman spectroscopy and thermogravimetry) and the determination of thermal conductivity and thermal resistance by the heat flow meter method, carried out at CECOVI (UTN Santa Fe). Each material was compared with its counterpart from the other country (BC BR with BC AR and BCC BR with BCC AR), and the conclusions are presented below according to the specific objectives of the research.

First, the limitations that define the scope of the results should be noted: the Brazilian ceramic blocks could not be tested for thermal conductivity, as they broke during transport to the laboratory in Argentina; for the Brazilian concrete, conductivity was determined only on flat slabs, without testing the hollow block; and each material corresponds to a single commercial batch per country. Thus, the thermal comparison between the ceramic block and the concrete block could only be made with the Argentine blocks.

Macroscopic properties (objective ii). Among the ceramic blocks, BC BR was about 21% denser than BC AR (2,072.94 kg/m³ vs. 1,718 kg/m³), but absorbed about 51% more water (22.67% vs. 15%) and was only 20% stronger (1.44 MPa vs. 1.2 MPa), a result that contradicts the expectation that higher density implies lower porosity. Among the concrete blocks, BCC BR was about 11% denser than BCC AR (2,191.04 kg/m³ vs. 1,980 kg/m³) and absorbed less water (5.12% vs. 8%), a behavior consistent with the relationship between density and porosity; however, BCC AR showed a compressive strength almost three times higher (6.9 MPa vs. 2.33 MPa) and much lower scatter (CV of 0.84% vs. 23.88%). From a standards perspective, the compressive strength of BC BR was below the minimum of 1.5 MPa required by NBR 15270-1 (ABNT, 2023), which calls for attention to the technological control of this material; BCC BR reached the reference value of 2.0 MPa adopted for non-load-bearing blocks in NBR 6136 (ABNT, 2016), and BCC AR met the minimum compressive strength requirement of IRAM 11561-2 (IRAM, 2018) for non-load-bearing blocks.

Microstructural characterization and correlation with macroscopic properties (objectives iii and iv). In the ceramic blocks, SEM, Raman spectroscopy and thermogravimetry indicated that both materials share the same performance-limiting mechanism, the incomplete consolidation of the clay particles during firing, with similar mineral phases (hematite, quartz and anatase) and high thermal stability between 25 °C and 600 °C. The type of clay and the mix composition influence porosity, but this effect is minimized by firing, so that the difference between the two blocks manifests mainly in the connectivity of the pore network: open and interconnected pores in BC BR, which help explain its higher water absorption, and larger but less interconnected voids in BC AR. In the concrete blocks, SEM showed a more continuous cementitious matrix in BCC AR and localized microcracks in BCC BR, and thermogravimetry recorded, in BCC AR, a higher mass loss between 450 °C and 600 °C, consistent with the dehydroxylation of portlandite; since this phase was not identified by Raman in this material, the hypothesis of a more advanced degree of hydration requires confirmation. The higher water absorption of BCC AR does not result from greater hydration and may be related to the mix proportions, the aggregate grading or the compaction of the blocks. This evidence, together with the lower scatter in strength, indicates that the mechanical strength of the concretes evaluated was associated with the quality and uniformity of the cementitious matrix rather than with apparent density. In both families of materials, apparent density proved to be an insufficient indicator of performance, which confirms the importance of microstructural characterization for interpreting macroscopic tests.

Thermal performance. Among the Argentine blocks, the only ones for which both types could be tested as hollow units, the ceramic block showed a mean thermal resistance of 0.348 m²·K/W, practically twice that obtained for the concrete block (0.178 m²·K/W), despite its smaller thickness. This result is consistent with the lower density and higher porosity of the ceramic matrix, although the geometry of the cavities of each block also contributes to the difference. For the Brazilian blocks, the comparison between ceramic and concrete remains open. In the dense concrete matrix, thermal conductivity was similar in the two countries (0.939 W/m·K in Brazil and 0.979 W/m·K in Argentina), despite the marked differences in mechanical strength, which indicates that the microstructural differences between the concretes had little effect on the thermal performance of this matrix. It should be noted that the thermal stability observed in thermogravimetry refers to the behavior of the material under

heating, and not to its performance as an insulator, which is assessed by thermal conductivity and thermal resistance.

Standard values and inputs for standardization. The values tabulated by IRAM 11601 (IRAM, 2004) proved very close to those measured, with a deviation of less than 1% for the Argentine ceramic block and concrete matrix, whereas ABNT NBR 15220-2 (ABNT, 2024) adopts for concrete a conductivity of 1.400 W/m·K, between 43% and 49% higher than the means measured in this study. The exclusive use of this tabulated value, without laboratory characterization, tends to overestimate heat transfer through dense concrete elements. Furthermore, the differences observed between materials with equivalent construction purposes indicate that transferring reference values from one country to another without an experimental basis may lead to specifications unsuited to the local context.

In light of these results, this research presents the following inputs for the revision of national standards and for the development of a future Mercosur standard (NM) on the thermal performance of walls:

i. Revision of the thermal conductivity values tabulated in ABNT NBR 15220-2 based on tests of regionally produced materials, following the example of the good agreement observed between the measured values and those tabulated by IRAM 11601;

ii. Harmonization of the methods for determining the thermal properties of materials between the two countries, based on existing standards such as IRAM 1860 and ABNT NBR 15220-5 and on the international reference standards (ASTM C518 and ISO 8301);

iii. Incorporation of acceptance quality control requirements for wall components, including water absorption and compressive strength tests with harmonized criteria between the countries.

In the Brazilian case, this control can rely on existing instruments, such as the Brazilian Program for Quality and Productivity in Housing (PBQP-H), whose Qualification System for Companies of Materials, Components and Building Systems (SiMaC) maintains Sectoral Quality Programs (PSQ) for ceramic blocks and for hollow concrete blocks, which periodically assess manufacturers' compliance with technical standards (Brasil, [20--]). The fact that BC BR did not reach the minimum strength required by NBR 15270-1 reinforces the importance of prioritizing products from

manufacturers qualified in these programs in the specification and acceptance of wall components.

In addition, the review of standards presented in Chapter 3, although not derived directly from the tests performed, points to the relevance of:

iv. Thermal transmittance limit values differentiated by bioclimatic zone and by season, as already adopted by IRAM 11605;

v. Hygrothermal verification requirements for the prevention of surface and interstitial condensation in external walls;

vi. Integration between the energy efficiency rating and labeling systems for buildings of the two countries, such as IRAM 11900 in Argentina and the Brazilian Building Labeling Program (PBE Edifica) (INMETRO, [20--]) in Brazil.

In summary, the results indicate that the performance of non-load-bearing blocks is influenced not only by the type of material but also by the raw material and the production process of each region: the effect of replacing the ceramic block with the concrete block was different in the two countries, with a strength gain of 62% in Brazil and 475% in Argentina, and a reduction in water absorption of 77% and 47%, respectively. Thus, the choice between the materials analyzed should not be based solely on mechanical and economic criteria, but should also consider the climatic context, the exposure conditions and the desired thermal performance, which reinforces regional experimental characterization as an indispensable step in the specification of wall materials.

Finally, considering the results as a whole, the Argentine blocks generally performed more favorably than the Brazilian ones. Among the ceramic blocks, BC AR absorbed about 34% less water than BC BR (15% vs. 22.67%) and showed lower scatter in density and absorption, although its compressive strength was slightly lower (1.2 MPa vs. 1.44 MPa), with both below the minimum of 1.5 MPa of the respective standards. Among the concrete blocks, BCC AR achieved the best mechanical performance of the entire set, with a strength almost three times higher than that of BCC BR and the lowest scatter among the materials studied, albeit with higher water absorption (8% vs. 5.12%). Since materials with the same construction purpose behaved differently in the two countries, it is concluded that the raw material available in each region, the manufacturing method and local production practices were determining factors for the performance of the blocks, which reinforces the need for experimental characterization of materials in their production context.

This work contributes to research on construction materials focused on thermal performance and energy efficiency, a strategic dimension for the sustainable development of Latin America, and can contribute to the Sustainable Development Goals of the UN 2030 Agenda: by supporting the specification of walls with better thermal performance, favoring occupant comfort and reducing dependence on active air conditioning (SDG 3 and SDG 7); by encouraging innovation and technological control in construction (SDG 9); and by supporting more sustainable cities and the reduction of CO_2 emissions associated with the energy consumption of buildings (SDG 11, SDG 12 and SDG 13).

The institutional cooperation between UFJF and UTN Santa Fe, which provided the methodological foundation for this research, is a model of techno-scientific rapprochement with potential for replication in other Mercosur contexts, strengthening Latin American research networks and fostering the production of knowledge applied to the real demands of regional construction.

As prospects for future research, the following are recommended: determination of the thermal conductivity of the Brazilian ceramic blocks and hollow concrete blocks by the same heat flow meter method, with replacement of the specimens damaged in transport; evaluation of the influence of moisture and mean test temperature on thermal conductivity; extension of thermogravimetry up to about 1,000 °C to evaluate carbonate decomposition; quantification of phases by X-ray diffraction and determination of porosity by mercury intrusion; monitoring of the thermal performance of full-scale wall prototypes under the climatic conditions of the two cities; inclusion of other wall materials and expansion of sampling to other batches and manufacturers; and extension of the comparative analysis to other Mercosur countries, expanding the regional database needed to consolidate a unified technical standard.

It is also recommended that the comparative methodology adopted in this research be extended to other Latin American countries beyond Mercosur, such as Chile, Peru, Colombia and Mexico, which encompass a great diversity of climates, raw materials and building traditions. Including new countries would make it possible to verify whether the influence of raw materials and regional production processes observed between Brazil and Argentina recurs in other contexts, as well as to expand the experimental database on the thermal and mechanical performance of Latin American wall components. This expansion could be made possible through cooperation networks between universities and research centers in the region, along

the lines of the partnership between UFJF and UTN Santa Fe, contributing to the construction of common technical references and to standard harmonization at the continental scale.

7 REFERENCES

ASSOCIAÇÃO BRASILEIRA DE NORMAS TÉCNICAS. **NBR 6136: Blocos vazados de concreto simples para alvenaria – Requisitos.** Rio de Janeiro: ABNT, 2016.

ASSOCIAÇÃO BRASILEIRA DE NORMAS TÉCNICAS. NBR 12118: Blocos vazados de concreto simples para alvenaria – Métodos de ensaio. Rio de Janeiro: ABNT, 2013.

ASSOCIAÇÃO BRASILEIRA DE NORMAS TÉCNICAS. **NBR 15575-4: Edificações habitacionais – Desempenho – Parte 4:** Requisitos para os sistemas de vedações verticais internas e externas – SVVIE. Rio de Janeiro: ABNT, 2021.

ASSOCIAÇÃO BRASILEIRA DE NORMAS TÉCNICAS. **NBR 15270-1: Componentes cerâmicos – Blocos** e tijolos para alvenaria. Rio de Janeiro: ABNT, 2023.

ASSOCIAÇÃO BRASILEIRA DE NORMAS TÉCNICAS**. NBR 15270-2**: Componentes cerâmicos – Blocos e tijolos para alvenaria – Parte 2: Métodos de ensaios. Rio de Janeiro: ABNT, 2017.

ASSOCIAÇÃO BRASILEIRA DE NORMAS TÉCNICAS. **NBR 15220-2: Desempenho térmico** de edificações – Parte 2: Componentes e elementos construtivos das edificações – Resistência e transmitância térmica – Métodos de cálculo. Rio de Janeiro: ABNT, 2024.

ASSOCIAÇÃO BRASILEIRA DE NORMAS TÉCNICAS. **NBR 15220-3: Desempenho térmico de edificações – Parte 3:** Zoneamento bioclimático por desempenho. Rio de Janeiro: ABNT, 2024.

ASSOCIAÇÃO BRASILEIRA DE NORMAS TÉCNICAS. **NBR 15220-5: Desempenho térmico** de edificações – Parte 5: Medição da resistência térmica e da condutividade térmica pelo método fluximétrico. Rio de Janeiro: ABNT, 2005.

ASSOCIAÇÃO BRASILEIRA DE NORMAS TÉCNICAS. **NBR 15575-1: Edificações habitacionais – Desempenho – Parte 1: Requisitos gerais.** Rio de Janeiro: ABNT, 2024.

ALHADDAD, M. A.; JUN, Z. T. A. Comparative Study of the Thermal Comfort of Different Building Materials in Sana'a. **American Journal of Engineering and Applied Sciences**, 2013. Available at: https://thescipub.com/abstract/ajeassp.2013.20.24. Accessed on: 5 Jan. 2026.

AMERICAN SOCIETY FOR TESTING AND MATERIALS. **ASTM C518-21**: Standard test method for steady-state thermal transmission properties by means of the heat flow meter apparatus. West Conshohocken: ASTM International, 2021. Accessed on: 5 Jan. 2026.

ASTM INTERNATIONAL. **ASTM C518-21**: Standard test method for steady-state thermal transmission properties by means of the heat flow meter apparatus. West Conshohocken: ASTM International, 2021.

ASTM INTERNATIONAL. **ASTM E967-18**: Standard test method for temperature calibration of differential scanning calorimeters and differential thermal analyzers. West Conshohocken: ASTM International, 2018.

ASTM INTERNATIONAL. **ASTM E1131-20**: Standard test method for compositional analysis by thermogravimetry. West Conshohocken: ASTM International, 2020.

ASTM INTERNATIONAL. **ASTM E1840-96 (2022)**: Standard guide for Raman shift standards for spectrometer calibration. West Conshohocken: ASTM International, 2022.

ASTM INTERNATIONAL. **ASTM E2529-16**: Standard guide for testing the resolution of a Raman spectrometer. West Conshohocken: ASTM International, 2016.

BALAJI, N. C.; MANI, M.; REDDY, B. V. V. Discerning heat transfer in building materials. Energy Procedia, v. 54, p. 654–668, 2014. DOI: 10.1016/j.egypro.2014.07.307. Available at: https://doi.org/10.1016/j.egypro.2014.07.307. Accessed on: 5 Jan. 2026.

BARBOSA, P. G.; AGUILAR, M. T. P.; SALES, R. D. B. C. Conforto térmico do ambiente construído, eficiência energética e difusividade térmica: um estudo interdisciplinar que envolve o Design. **Pensamento em design**, Belo Horizonte, v. 1, 2021. Available at: https://revista.uemg.br/index.php/pensemdes/article/view/5914/3591. Accessed on: 29 Mar. 2025.

BARETTA, M. “À son Excellence Monsieur le Gouverneur”: inmigración, escritura y formación del Estado (Santa Fe, 1860-1887). **Revista Electrónica de Fuentes y Archivos**, 2024. Accessed on: 12 Apr. 2025.

BARRIENTOS SANTINI, G.; CARRARA, J. M. **Análisis comparativo de la conductividad térmica en materiales de construcción mediante el método de flujo de calor**. Santa Fe: CECOVI, UTN Facultad Regional Santa Fe; Juiz de Fora: UFJF, 2026. Accessed on: 25 Sept. 2026.

BARTOLOMEU, M. C. A cafeicultura e a Estrada União e Indústria. **Revista da Rede Brasileira de História da Geografia, 2019.** Accessed on: 12 Apr. 2025.

BHAMARE, D. K.; RATHOD, M. K.; BANERJEE, J. Passive cooling techniques for building and their applicability in different climatic zones—The state of art. **Energy and Buildings**, v. 198, p. 467-490, set. 2019. Available at: https://www.sciencedirect.com/science/article/abs/pii/S0378778819300210. Accessed on: 18 July 2025.

BRÍGITTE, G. T. N.; RUSCHEL, R. C. Modelo de informação da construção para o projeto baseado em desempenho: caracterização e processo. **Ambiente Construído**, v. 16, 2016. Accessed on: 29 Mar. 2025.

BUENO, G. M.; GONZALEZ, M. A. S.; TUTIKIAN, B. F.; FERREIRA, J. S. Verificação das condições acústicas de habitação de interesse social de acordo com a norma brasileira NBR 15575. **Revista AIDIS de ingeniería y ciencias ambientales: Investigación, desarrollo y práctica**, 2019. Available at: http://www.journals.unam.mx/index.php/aidis/article/view/60851. Accessed on: 5 Jan. 2026.

CAVALCANTI, F. Impacto da absortância e transmitância das fachadas na eficiência energética e conforto térmico para habitação de interesse social. **Paranoá, Brasília, 2020.** Available at: https://periodicos.unb.br/index.php/paranoa/article/view/32043/28020. Accessed on: 18 July 2025.

CARNEIRO, P. C. S.; OLIVEIRA, R. D. Desempenho termo acústico de sistemas construtivos: estudo de ferramentas aplicáveis a verificação da conformidade de habitação multifamiliar segundo requisitos da NBR 15.575/2013. **Matéria**, v. 25, p. 24, 2020. Available at: https://www.scielo.br/j/rmat/a/ZSfQKtNpqGkYG4LXJkZrSxj/abstract/?lang=pt. Accessed on: 29 Mar. 2025.

CONSELHO BRASILEIRO DE CONSTRUÇÃO SUSTENTÁVEL (CBCS). Posicionamento CBCS: eficiência energética no ambiente construído. CBCS, Comitê Temático de Energia, 2015. Accessed on: 5 Jan. 2026.

COLETTI, C.; CULTRONE, G.; MARITAN, L.; MAZZOLI, C. Combined multi-analytical approach for study of pore system in bricks: how much porosity is there? Materials Characterization, New York, v. 121, p. 82-92, 2016. Accessed on: 10 Nov. 2026.

CULTRONE, G. et al. Influence of mineralogy and firing temperature on the porosity of bricks. Journal of the European Ceramic Society, Oxford, v. 24, n. 3, p. 547-564, 2004. Accessed on: 10 Nov. 2026.

CHVATAL, K. M. S. Avaliação do procedimento simplificado da NBR 15575 para determinação do nível de desempenho térmico de habitações. **Ambiente Construído**, 2014. Available at: https://www.scielo.br/j/ac/a/KtKYFm865hxXwPvpfMcBncH/abstract/?lang=pt. Accessed on: 29 Mar. 2025.

CRUZ, M. C. L. D. Conforto Térmico nas Edificações: Materiais e Técnicas Construtivas. Um estudo comparativo entre a cidade de Ouro Preto - Brasil e Porto - Portugal. **Arq.urb**, v. 27, 2020. Available at: https://revistaarqurb.com.br/arqurb/article/view/404/366. Accessed on: 29 Mar. 2025.

DURAKOVIC, B.; YILDIZ, G.; YAHIA, M. E. Comparative Performance Evaluation of Conventional and Renewable Thermal Insulation Materials Used in Building Envelops. **Tehnički vjesnik**, v. 27, 2020. Accessed on: 5 Jan. 2026.

EL-BICHRI, F.-Z.; SOBHY, I.; BOUCHEFRA, I.; BENHAMOU, B.; CHEHOUANI, H.; MGHAZLI, M. O. Assessment of the impact of construction materials on the building's thermal behaviour and indoor thermal comfort in a hot and semi-arid climate. Advances in Building Energy Research, v. 16, p. 711–735, 2022. DOI: 10.1080/17512549.2022.2096692. Available at: https://doi.org/10.1080/17512549.2022.2096692. Accessed on: 5 Jan. 2026.

ELIAS-OZKAN, S.; SUMMERS, F.; SURMELI, A. N.; YANNAS, S. **A Comparative Study of the Thermal Performance of Building Materials**. In: CONFERENCE ON PASSIVE AND LOW ENERGY ARCHITECTURE, 23., 2005, Geneva. Proceedings [...]. [S. l.: s. n.], 2006. Accessed on: 5 Jan. 2026.

FATI, A. O.; BONKANEY, A. L.; OUEDRAOGO, S.; KY, S. M. T.; LEWAMY, M.; BATHIEBO, D. J. The impact of local materials on the improvement of the thermal comfort in building. Current Journal of Applied Science and Technology, v. 39, n. 15, p. 22–35, 16 jun. 2020. DOI: 10.9734/cjast/2020/v39i1530713. Available at: https://doi.org/10.9734/cjast/2020/v39i1530713. Accessed on: 5 Jan. 2026.

FERREIRA, C. D. C. M.; SANCHES, F. O.; OLIVEIRA, T. A.; VIANNA, Y. C. G.; TAVARES, C. M. G. **Clima de Juiz de Fora**: 50 anos de dados meteorológicos. Juiz de Fora: Editora UFJF, 2023. 82 p. Available at: https://www2.ufjf.br/editora/wp-content/uploads/sites/113/2023/10/Clima-de-Juiz-de-Fora-Editora-UFJF.pdf. Accessed on: 29 Mar. 2025.

FILHO, B. F. D. S. **Estudo das propriedades térmicas de diferentes tijolos. 2023. 61 f. Dissertação (Mestrado) – Universidade** de Cuiabá, Cuiabá, 2023. Accessed on: 5 Jan. 2026.

FÖLDVÁRI, M. **Handbook of thermogravimetric system of minerals and its use in geological practice**. Budapest: Geological Institute of Hungary, 2011. (Occasional Papers of the Geological Institute of Hungary, v. 213). Accessed on: 10 Nov. 2026.

GOMES, E. G. S.; MELO, A. B. D. Caracterização do fluxo de calor em alvenaria com blocos EVA. **PARC Pesquisa em Arquitetura e Construção**, v. 9, 2018. Accessed on: 29 Mar. 2025.

WORLD BANK GROUP. Climate Change Knowledge Portal: Argentina. World Bank Group, 2021. Accessed on: 5 Jan. 2026.

GUARDA, E. L. A. D.; DURANTE, L. C.; CALLEJAS, I. J. A. Parâmetros climáticos para simulação de desempenho térmico segundo a NBR 15.575. **PARC: Pesquisa em Arquitetura e Construção**, v. 11, 2020. Available at: https://periodicos.sbu.unicamp.br/ojs/index.php/parc/article/view/8655374. Accessed on: 29 Mar. 2025.

INSTITUTO BRASILEIRO DE GEOGRAFIA E ESTATÍSTICA. **Cidades e Estados**. Rio de Janeiro: IBGE, 2022. Available at: https://www.ibge.gov.br/cidades-e-estados. Accessed on: 29 Mar. 2025.

IJJADA, N.; NAYAKA, R. R. Review on properties of some thermal insulating materials providing more comfort in the building. **Materials Today: Proceedings**, 2022. Accessed on: 13 Apr. 2025.

INSTITUTO NACIONAL DE ESTADÍSTICA Y CENSOS (INDEC). Resultados del Censo 2022. Buenos Aires: INDEC, 2022. Accessed on: 5 Jan. 2026.

INSTITUTO NACIONAL DE METROLOGIA, QUALIDADE E TECNOLOGIA (INMETRO). **Programa Brasileiro de Etiquetagem de Edificações – PBE Edifica**. Brasília: Inmetro, [20--]. Available at: https://pbeedifica.com.br. Accessed on: 26 Sept. 2026.

INSTITUTO ARGENTINO DE NORMALIZACIÓN Y CERTIFICACIÓN (IRAM). **IRAM 1860**: Materiales aislantes térmicos – Método de ensayo de las propiedades de transmisión térmica en régimen estacionario mediante el aparato medidor de flujo de calor. Buenos Aires: IRAM, 2002.

INSTITUTO ARGENTINO DE NORMALIZACIÓN Y CERTIFICACIÓN (IRAM). I**RAM 11561-2**: Bloques de hormigón no portantes – Requisitos. Buenos Aires: IRAM, 2018.

INSTITUTO ARGENTINO DE NORMALIZACIÓN Y CERTIFICACIÓN (IRAM). **IRAM 11561-4**: Bloques de hormigón – Métodos de ensayo. Buenos Aires: IRAM, 2018.
INSTITUTO ARGENTINO DE NORMALIZACIÓN Y CERTIFICACIÓN (IRAM). IRAM 11605: Acondicionamiento térmico de edificios – Condiciones de habitabilidad en edificios. Valores máximos de transmitancia térmica en cerramientos opacos. Buenos Aires: IRAM, 2002.

INSTITUTO ARGENTINO DE NORMALIZACIÓN Y CERTIFICACIÓN (IRAM). **IRAM 11601:** Aislamiento térmico de edificios – Métodos de cálculo – Propiedades térmicas de los componentes y elementos de construcción en régimen estacionario. Buenos Aires: IRAM, 2004.

INSTITUTO ARGENTINO DE NORMALIZACIÓN Y CERTIFICACIÓN (IRAM). **IRAM 11900**: Prestaciones energéticas en viviendas – Método de cálculo y etiquetado de eficiencia energética. Buenos Aires: IRAM, 2019.

INSTITUTO ARGENTINO DE NORMALIZACIÓN Y CERTIFICACIÓN (IRAM). **IRAM 12566-1**: Ladrillos cerámicos macizos para la construcción de muros – Requisitos. Buenos Aires: IRAM, 2005.

INSTITUTO ARGENTINO DE NORMALIZACIÓN Y CERTIFICACIÓN (IRAM). **IRAM 12566-2**: Ladrillos y bloques cerámicos, perforados y huecos para la construcción de muros – Requisitos. Buenos Aires: IRAM, 2005.

INSTITUTO ARGENTINO DE NORMALIZACIÓN Y CERTIFICACIÓN (IRAM). **IRAM 12586**: Ladrillos y bloques cerámicos para la construcción de muros – Método de ensayo de resistencia a la compresión. Buenos Aires: IRAM, 2004.

INSTITUTO ARGENTINO DE NORMALIZACIÓN Y CERTIFICACIÓN (IRAM). **IRAM 12593**: Ladrillos y bloques cerámicos para la construcción de muros – Métodos de ensayo de densidad aparente y absorción de agua. Buenos Aires: IRAM, 2004.

INTERNATIONAL ORGANIZATION FOR STANDARDIZATION. **ISO 8301**: Thermal insulation – Determination of steady-state thermal resistance and related properties – Heat flow meter apparatus. Geneva: ISO, 1991.
KAMAL, M. A. Material Characteristics and Building Physics for Energy Efficiency. **Key Engineering Materials**, v. 666, 2015. Accessed on: 13 Apr. 2025.

International Organization for Standardization. **ISO 8301**: Thermal insulation – Determination of steady-state thermal resistance and related properties – Heat flow meter apparatus. Geneva: ISO, 1991.

ISO. **ISO 11358-1**: Plastics – Thermogravimetry (TG) of polymers – Part 1: General principles. Geneva: ISO, 2022.

International Organization for Standardization. **ISO 16700**: Microbeam analysis – Scanning electron microscopy – Guidelines for calibrating image magnification. Geneva: ISO, 2016.

International Organization for Standardization. **ISO 22493**: Microbeam analysis – Scanning electron microscopy – Vocabulary. Geneva: ISO, 2014.

KLAMT, R. A.; SCHNEIDER, M.; FAURO, D.; JÚNIOR, B. H. Uso do isopainel para controle do conforto térmico em edificações. **Revista de Engenharia e Tecnologia**, v. 16, p. 13, 29 maio 2024. Available at: https://revistas.uepg.br/index.php/ret/article/view/22943/209209218644. Accessed on: 29 Mar. 2025.

KOHL, F.; SILVA, T. L. D.; RIBEIRO, L. A. Análise de eficiência energética em edificação de concreto armado moldado in loco. **Revista de arquitetura IMED**, v. 12, p. 12, 2023. Available at: https://seer.atitus.edu.br/index.php/arqimed/article/view/4960/3277. Accessed on: 29 Mar. 2025.

KUMAR, D.; ALAM, M.; ZOU, P. X. W.; SANJAYAN, J. G.; MEMON, R. A. Comparative analysis of building insulation material properties and performance. **Renewable and Sustainable Energy Reviews**, v. 131, 2020. Accessed on: 13 Apr. 2025.

LAMBERTS, R. **Desempenho térmico de edificações – Aula 12: Diretrizes construtivas para habitações no Brasil – NBR 15220.** Florianópolis: Universidade Federal de Santa Catarina, 2016. Accessed on: 5 Jan. 2026.

LANZET, A. **Acondicionamiento higrotérmico de edificios**. Buenos Aires, 2013. 41 p. Available at: https://procesosconstructivos.wordpress.com/wp-content/uploads/2013/02/ley-13059-manual_ac_higrotermico.pdf. Accessed on: 5 Jan. 2026.

MANSOURI, K.; LEILA, S. Investigating the effectiveness of the building's envelope materials in hot and arid climates to achieve indoor thermal comfort. **International Journal of Advanced Natural Sciences and Engineering Researches**, v. 7, n. 7, p. 120–127, 2023. DOI: 10.59287/ijanser.1346. Available at: https://as-proceeding.com/index.php/ijanser/article/view/1346. Accessed on: 5 Jan. 2026.

MARTINS, T. A. D. L.; BITTENCOURT, L. S.; KRAUSE, C. M. D. L. B. Contribuição ao zoneamento bioclimático brasileiro: reflexões sobre o semiárido nordestino. **Ambiente Construído**, v. 12, 2012. Accessed on: 29 Mar. 2025.

MILANO, A. La élite santafesina en la segunda mitad del siglo xvii y. **Cuadernos de Historia**, Córdoba, 2011. Available at: https://revistas.unc.edu.ar/. Accessed on: 5 Jan. 2026.

NASR, Y.; ZAKHEM, H. E.; HAMAMI, A. E. A.; BACHAWATI, M. E.; BELARBI, R. Comprehensive Review of Innovative Materials for Sustainable. **Energies**, 2023. Accessed on: 13 Apr. 2025.

NETTO, G. R.; CZAJKOWSKI, J. D. Comparación entre las normas de desempeño térmico edilício de Argentina y Brasil. **Ambiente Construído**, v. 16, 2016. Available at: https://www.scielo.br/j/ac/a/VFhXrwx5pBPwRYydNXXFw6s/?lang=es. Accessed on: 29 Mar. 2025.

NUNES, V. D. L.; HIPPERT, M. A. S.; CARVALHO, A. R.; RUBIM, D. F. A implantação da norma NBR 15575 e seu impacto no setor de construção civil. **PARC Pesquisa em Arquitetura e Construção**, Campinas, 2021. Available at: https://periodicos.sbu.unicamp.br/ojs/index.php/parc/article/view/8656159. Accessed on: 29 Mar. 2025.

OLIVEIRA, C. C. D.; RUPP, R. F.; GHISI, E. Influência da umidade do ar no conforto térmico de usuários de edificações de escritórios em Florianópolis/SC. **Ambiente Construído**, Porto Alegre, v. 20, p. 15, 5 out. 2020. Available at: https://www.scielo.br/j/ac/a/y4TZG8X6GfvpZZMDhr8TsBj/. Accessed on: 29 Mar. 2025.

OLIVEIRA, D. E. D.; ASSIS, D. C.; PIMENTEL, F. D. O.; FERREIRA, C. C. M.; VIANNA, Y. C. G. Estudo dos ventos na área central da cidade de Juiz de Fora (MG): um ensaio da espacialização de seus fluxos. **Revista do Programa de Pós-Graduação em Geografia**, 2017. Available at: https://ojs.ufgd.edu.br/index.php/entre-lugar/article/view/8087. Accessed on: 29 Mar. 2025.

OLIVEIRA, L. E. P. Cotidiano, associativismo e reivindicações operárias em Juiz de Fora nos anos 1920. 2020. Available at: https://www.semanticscholar.org/paper/COTIDIANO%2C-ASSOCIATIVISMO-E-

REIVINDICA%C3%87%C3%95ES-EM-JUIZ-Oliveira/d5e7d1683547fea4d805db492d81d15300e114a3. Accessed on: 12 Apr. 2025.

OLIVEIRA, P. A. D.; LUNARDI, D. G. Influência da envoltória no desempenho termoenergético de edificações institucionais no semiárido. **PARC: Pesquisa em Arquitetura e Construção**, v. 9, 2018. Available at: https://doi.org/10.20396/parc.v9i4.8651048. Accessed on: 29 Mar. 2025.

ORTLEPP, R.; SATANOVA, Z. Influence of regional context in building design on the transferability of material indicators: A case study of a residential building type in Kazakhstan and Germany**. Civil Engineering Papers**, v. 8, n. 3-4, p. 71-80, 2025. DOI: 10.1002/cepa.3339. Available at: https://onlinelibrary.wiley.com/doi/10.1002/cepa.3339. Accessed on: 5 Jan. 2026.

PAGNOSSIN, E. M.; BURIOL, G. A.; GRACIOLLI, M. D. A. Influência dos elementos meteorológicos no conforto térmico humano: bases biofísicas. **Disciplinarum Scientia, Santa Maria**, v. 2, p. 13, 2001. Available at: https://periodicos.ufn.edu.br/index.php/disciplinarumS/article/view/803/747. Accessed on: 29 Mar. 2025.

PEREIRA, C.; SOUZA, R.; VELOSO, A. C.; CARVALHO, F.; SARAIVA, L.; PASCOAL, L.; PINHEIRO, B. **Conforto térmico em sala de informática:** conforto adaptativo pela ASHRAE 55 x conforto relatado pelos usuários. In: ENCONTRO NACIONAL DE TECNOLOGIA DO AMBIENTE CONSTRUÍDO, 18., 2020. Anais. 2020. Accessed on: 5 Jan. 2026.

PREFEITURA MUNICIPAL DE JUIZ DE FORA (PMJF). Características da cidade. Juiz de Fora: PJF, 2018. Available at: https://www.pjf.mg.gov.br/institucional/cidade/caracteristicas.php. Accessed on: 29 Mar. 2025.

UNITED NATIONS ENVIRONMENT PROGRAMME (UNEP). Global Status Report for Buildings and Construction. Nairobi: UNEP, 2024. Accessed on: 5 Jan. 2026.

QIN, Z.; LI, M.; FLOHN, J.; HU, Y. Thermal management materials for energy-efficient and sustainable future buildings. **Chemical Communications**, 2021. Accessed on: 13 Apr. 2025.

SANTOS, J. C. P. D.; KOTHE, K. K.; MOHAMAD, G.; VAGHETTI, M. A. O.; RIZZATTI, E. Comportamento térmico de fechamentos em alvenaria estrutural para a Zona Bioclimática 2 brasileira. **Matéria**, v. 20, p. 18, 2015. Available at: https://www.scielo.br/j/rmat/a/FcfDnYQNbMDFtmYpBwkRBxC/?lang=pt. Accessed on: 29 Mar. 2025.

SANTOS, W. N. D. Métodos transientes de troca de calor na determinação das propriedades térmicas de materiais cerâmicos: I - o método de pulso de energia. **Cerâmica**, v. 319, set. 2008. Accessed on: 29 Mar. 2025.

SANTOS, P. S. **Ciência e tecnologia de argilas**. 2. ed. São Paulo: Edgard Blücher, 1989. v. 1. Accessed on: 10 Nov. 2026.

SCHILLER, G.; MIATTO, A.; GRUHLER, K.; ORTLEPP, R.; DEILMANN, C.; TANIKAWA, H. Transferability of material composition indicators for residential buildings: a conceptual approach based on a German–Japanese comparison. **Journal of Industrial Ecology**, v. 23, n. 4, p. 796–807, 2019. DOI: 10.1111/jiec.12817. Available at: https://doi.org/10.1111/jiec.12817. Accessed on: 5 Jan. 2026.

SERVICIO METEOROLÓGICO NACIONAL (SMN). Servicio Meteorológico Nacional. Buenos Aires: SMN, 2024. Available at: https://www.argentina.gob.ar/smn. Accessed on: 8 Oct. 2024.

SOLIMAN, A.; HAFEEZ, G.; ERKMEN, E.; GANESAN, T.; OUF, M.; HAMMAD, A.; EICKER, U.; MOSELHI, O. Innovative construction material technologies for sustainable and resilient civil infrastructure. **Materials Today: Proceedings**, Montreal, v. 60, 2022. Available at: https://www.sciencedirect.com/science/article/abs/pii/S2214785322002929. Accessed on: 29 Mar. 2025.

SORGATO, M. J.; MARINOSKI, D. L.; MELO, A. P.; LAMBERTS, R. **Nota técnica referente à avaliação para a norma de desempenho NBR 15575 em consulta pública. Florianópolis: Universidade Federal de Santa Catarina, 2012.** Accessed on: 5 Jan. 2026.

WEATHER SPARK. Clima e condições **meteorológicas médias em Santa Fe de la Vera Cruz no ano todo. Weather Spark, 2018.** Accessed on: 5 Jan. 2026.

SURYO, M. S. Influence of Structure and Wall Materials on Building Thermal Performance. **KnE Social Sciences**, v. 3, n. 21, p. 521–534, 5 ago. 2019. DOI: 10.18502/kss.v3i21.4992. Available at: https://doi.org/10.18502/kss.v3i21.4992. Accessed on: 5 Jan. 2026.

TIGRE, A. L. **Eficiência energética em edifícios com fachada de vidro. Curitiba: Universidade Tecnológica Federal do Paraná, 2016.** Accessed on: 5 Jan. 2026.

UNITED NATIONS EDUCATIONAL, SCIENTIFIC AND CULTURAL ORGANIZATION (UNESCO). Recommendation on the Ethics of Artificial Intelligence. Paris: UNESCO, 2021. Available at: https://unesdoc.unesco.org/ark:/48223/pf0000381137. Accessed on: 21 June 2026.

VENTURINI, V. **Thermal condition of Santa Fe city – Argentina during the period 2013-2022. In: IEEE BIENNIAL CONGRESS OF ARGENTINA (ARGENCON), 2022. Proceedings. IEEE, 2022.** Accessed on: 5 Jan. 2026.

WIKIPEDIA. Santa Fe (Argentina). 2025. Available at: https://pt.wikipedia.org/wiki/Santa_F%C3%A9_(Argentina). Accessed on: 9 Apr. 2025.